CORRECTED 12 APRIL 2024; SEE ERRATUM

SCIENCE ADVANCES | RESEARCH ARTICLE

APPLIED SCIENCES AND ENGINEERING

Inhibiting sorting nexin 10 promotes mucosal healing through SREBP2-mediated stemness restoration of intestinal stem cells

Weilian Bao[1,2]†, Yan You[1]†, Jiahui Ni[1]†, Hui Hou[3], Jiaren Lyu[1], Guize Feng[1], Yirui Wang[1], Keyuan You[1], Sulin Zhang[3], Lijie Zhang[4], Xinyue Cao[1], Xu Wang[1], Haidong Li[1], Hong Li[1], Jiake Xu[5,6], Chenying Liu[7,8], Xiaomin Luo[3], Peng Du[7,8]*, Daofeng Chen[2]*, Xiaoyan Shen[1]*

Intestinal stem cell (ISC) is a promising therapeutic target for inflammatory bowel disease. Cholesterol availability is critical for ISC stemness. Low plasma cholesterol is a typical feature of Crohn's disease (CD); however, its impact on mucosal healing remains unclear. Here, we identified an essential role of sorting nexin 10 (SNX10) in maintaining the stemness of ISCs. SNX10 expression in intestinal tissues positively correlates with the severity of human CD and mouse colitis. Conditional SNX10 knockout in intestinal epithelial cells or ISCs promotes intestinal mucosal repair by maintaining the ISC population associated with increased intracellular cholesterol synthesis. Disassociation of ERLIN2 with SCAP by SNX10 deletion enhances the activation of SREBP2, resulting in increased cholesterol biosynthesis. DC-SX029, a small-molecule inhibitor of SNX10, was used to verify the druggable potential of SNX10 for the treatment of patients with CD. Our study provides a strategy for mucosal healing through SREBP2-mediated stemness restoration of ISCs.

INTRODUCTION

Loss of an integrated epithelial barrier leads to inappropriate translocation of gut luminal contents, commensal microbiota, and pathogenic microbes into the intestinal lamina propria and eventually induces intestinal inflammation and mucosa injury. Complete repair of the damaged mucosa clinically, referred to as mucosal healing, is a prognostic indicator for long-term relief and reduced surgical risk in patients with inflammatory bowel disease (IBD) according to clinical studies (*1*). Under physiological conditions, the intestinal epithelial cells (IECs) are replenished from intestinal stem cells (ISCs) residing in the basal crypts every 3 to 4 days to preserve a continuous mucosal barrier. While the damage of the epithelial layer by various factors including infection, radiation, ischemia, physical trauma, or immune-mediated injury promotes the repair process for restoring the barrier function of the epithelium, it requires proper spatial allocation and organization of ISCs under the regulation of molecules secreted by surrounding niches (*2*). Recent studies indicate that impaired ISC function in patients with Crohn's disease (CD) and mice models is responsible for its chronic, relapsing inflammation (*3*–*6*). Altered metabolic patterns in ISCs and associated niches are closely correlated with the aberrant function and activation of ISCs (*3*, *7*–*9*). It was reported that cholesterol synthesis in ISCs is essential for the maintenance of its function (*9*), and low blood cholesterol level is a typical feature of active CD (*10*–*12*). However, the contribution of altered cholesterol metabolism in ISCs to CD progression has not been disclosed.

Sorting nexin 10 (SNX10) belongs to the SNX family characterized by the presence of phox homology domain, which binds to phosphoinositide on membrane structure. Previous studies found that SNX10 locates on the endosome, lysosome, and endoplasmic reticulum (ER) and acts as an adaptor protein to mediate signaling transduction and intracellular protein trafficking (*13*–*15*). SNX10 has been identified as a key driver of intestinal inflammation in a functional genomics predictive network model based on three populations of patients with different stages of IBD (*16*). We previously described the critical role of SNX10 in mediating inflammatory response in macrophages, contributing to the development of colitis in mice (*17*, *18*). Other groups reported that SNX10 acts as an important regulator of lipid metabolism in immune cells and adipocytes (*19*–*23*). Here, we confirmed that SNX10-driven CD risk was closely associated with the impairment of intestinal epithelial barrier function. We found that SNX10 restricted the expansion and function of ISCs by limiting cholesterol biosynthesis both in vivo and ex vivo. We further demonstrated that SNX10 deletion promoted sterol regulatory element–binding protein 2 (SREBP2) cleavage by disassociating endoplasmic reticulum (ER) lipid raft associated 2 protein(ERLIN2) with sterol regulatory element-binding protein cleavage-activating protein (SCAP) on ER. Last, a previously identified SNX10 protein-protein interaction (PPI) inhibitor was used to verify the potential of SNX10 as a therapeutic target for IBD.

RESULTS

SNX10 expression in intestinal tissues positively correlates with the severity of CD

To understand the impact of SNX10 on CD, we first analyzed whole-genome transcriptome profiling data (GSE112366 dataset) from

[1]Department of Pharmacology and the Key Laboratory of Smart Drug Delivery Ministry of Education, School of Pharmacy, Fudan University, Shanghai, China. [2]Department of Natural Medicine, School of Pharmacy, Fudan University, Shanghai, China. [3]Drug Discovery and Design Center, State Key Laboratory of Drug Research, Shanghai Institute of Materia Medica, Chinese Academy of Sciences, Shanghai, China. [4]Department of Radiation Oncology, Fudan University Shanghai Cancer Center, Shanghai, China. [5]School of Biomedical Sciences, University of Western Australia, Perth, WA, Australia. [6]Shenzhen Institute of Advanced Technology, Chinese Academy of Sciences, Shenzhen, China. [7]Department of Colorectal and Anal Surgery, Xinhua Hospital, Shanghai Jiao Tong University School of Medicine, Shanghai, China. [8]Shanghai Colorectal Cancer Research Center, Shanghai, China.
*Corresponding author. Email: shxiaoy@fudan.edu.cn (X.S.); dfchen@shmu.edu.cn (D.C.); dupeng@xinhuamed.com.cn (P.D.)
†These authors contributed equally to this work.

patients with active CD (*24*). As shown in Fig. 1A, *SNX10* expression significantly increased in biopsy samples from patients with CD compared to healthy controls. Correlation analysis revealed a moderate positive correlation between *SNX10* expression and simple endoscopic score for CD, an index for disease severity (Fig. 1B). Data from another clinical study (GSE100833 dataset) showed that *SNX10* expression was higher in inflamed areas than noninvolved areas from the same intestinal segment (Fig. 1C). Among 141 IBD susceptible genes (*25*), 92 genes were positively correlated with SNX10 expression and 31 genes were negatively correlated with SNX10 expression ($r > 0.3$) (fig. S1A). The gene expression of current therapeutic targets for IBD was also positively correlated with *SNX10* expression (fig. S1B). Gene set enrichment analysis (GSEA) showed that multiple immune cell activation–related gene sets annotated by Gene Ontology (GO) Resource (geneontology.org) were enriched in the patients with high SNX10 expression (fig. S1C), while epithelial cell maintenance–related gene sets annotated by GO resource were enriched in the patients with low SNX10 expression (Fig. 1D). Immunofluorescence staining of surgically resected ileum from patients with CD showed a significant up-regulation of SNX10 in typical lesions (Fig. 1E), including crypt branching, crypt atrophy, and crypt abscess, especially, in infiltrating macrophages (fig. S1D). The contribution of SNX10 in macrophages to colitis has been discussed in our paper published previously (*17*). As inflammatory cell infiltration intensified, SNX10 high-expressing epithelial cells in crypts increased (Fig. 1F). These results indicate a crucial role of intestinal SNX10 in the pathological process of CD, associated with both macrophages and epithelial cells.

Intestinal epithelium SNX10 deletion alleviated DSS-induced colitis and mucosal injury

Similarly, the positive correlation between SNX10 and colitis severity is also exhibited in IBD animal models. In 2,4,6-trinitrobenzenesulfonic acid solution (TNBS)–induced mouse colitis (GSE35609 dataset) (*26*), *Snx10* expression increased with the prolongation of the disease course and reached its peak at day 14 (fig. S2A). In the colon of interleukin-10–deficient (*Il-10*$^{-/-}$) mice that spontaneously develop colitis at about 12 weeks of age (GSE27684 dataset) (*27*), *Snx10* expression was significantly higher than that in wild-type (WT) mice (fig. S2B). In the proximal and distal colon of dextran sulfate sodium (DSS)–induced colitis mice, SNX10 expression was positively correlated with the time of DSS exposure (figs. S2, C and D). Consistent with the results from clinic data, we also observed SNX10 staining enhanced increasingly in the lamina propria and epithelium of colon tissues following colitis development by DSS treatment (Fig. 2A). This result was confirmed by reverse transcription quantitative polymerase chain reaction (RT-qPCR) and Western blot (WB) performed on colonic epithelial cells (EPCAM^{+}CD45^{-}) (Fig. 2B and fig. S2E). To understand the impact of intestinal epithelium SNX10 on colitis, we further evaluated the effect of epithelial-specific deletion of *Snx10* on the development of IBD in mice. As shown in fig. S2F, the inserted loxp sites did not affect *Snx10* expression. *Snx10* IEC-specific knockout (KO) mice were obtained by crossing *Snx10*$^{fl/fl}$ mice with *Vil-Cre* mice (fig. S2G), and the efficiency of KO was confirmed by showing a significant reduction of SNX10 in the epithelial cells of *Snx10*$^{fl/fl}$;Cre^{+} (*Snx10*$^{\Delta IEC}$) mice compared to *Snx10*$^{fl/fl}$;Cre^{-} (WT) mice both at basal level and in IBD models (fig. S2H). Survival experiment showed that intestinal *Snx10* deficiency effectively elevated the survival rate of DSS-treated mice (Fig. 2C). Weight change (Fig. 2D) and disease activity index (DAI) score (fig. S2I) revealed a quicker recovery of *Snx10*$^{\Delta IEC}$ mice after 6-day modeling. Consistent with the symptoms, the colon shortening (Fig. 2E) and the elevated levels of pro-inflammatory cytokines in serum (fig. S2J) and tissues (Fig. 2F) were significantly ameliorated in *Snx10*$^{\Delta IEC}$ colitis mice. Hematoxylin and eosin (H&E) staining revealed that intestinal *Snx10* deficiency effectively alleviated inflammatory cell infiltration and tissue damage (Fig. 2G) and retained more intact and lengthened crypt structures (fig. S2, K and L) in colitis mice. Moreover, E-cadherin staining and intestinal permeability assays showed that barrier dysfunction was significantly ameliorated in *Snx10*$^{\Delta IEC}$ colitis mice (fig. S2, M and N). DSS-induced colitis is the classic epithelial injury–driven IBD model, which is suitable for studying repetitive tissue regeneration and wound healing after epithelial injury. However, the TNBS model more closely resembles human CD in terms of immunological features (*28*). Hence, we further investigated the phenotype of *Snx10*$^{\Delta IEC}$ mice in the TNBS model. As shown in Fig. 2, H and I, SNX10 deficiency effectively alleviated weight loss and shortened colon length in the TNBS model. Consistently, inflammatory cell infiltration, colonic patch hypertrophy, and elevated pro-inflammatory cytokines caused by TNBS were significantly reduced in *Snx10*$^{\Delta IEC}$ mice compared to WT mice (Fig. 2, J and K). Collectively, these data suggest that intestinal epithelium SNX10 plays a critical role in the pathological injury of mucosa barrier function and is the key factor to determine the severity and prognosis of IBD.

SNX10 deficiency enhanced the stemness of CBC stem cells and promoted the differentiation of secretory-lineage cells

The maintenance of intestinal mucosa barrier function relies on the self-renewal of IECs that are continually replenished by ISCs located at the crypt. Following self-renew, ISCs differentiate into absorptive and secretory-lineage cells for replacing constant cell loss (*29*). We observed a significantly increased staining of regeneration marker Ki67, and ISC marker AXIN2 in the colon tissues of *Snx10*$^{\Delta IEC}$ colitis mice, indicating a vigorous repairment of intestinal epithelium (Fig. 3, A and B). Immunostaining revealed that the recovered epithelial cells consisted of more goblet cells (Alcian blue^{+}) and tufts cells (COX1^{+}) while fewer absorptive cells (CAII^{+}) in *Snx10*$^{\Delta IEC}$ mice (fig. S3, A and B). We observed a similar recovery of Ki67^{+} cells and goblet cells in the TNBS model of *Snx10*$^{\Delta IEC}$ mice (fig. S3, C and D). Samples from patients with CD also showed that Ki67 staining decreased in the crypts of mildly inflamed areas compared to that of normal areas and was negatively correlated with SNX10 expression (Fig. 3C and fig. S3E). To confirm the role of *Snx10* in manipulating the stemness of ISCs, the mRNA levels of markers related to crypt base columnar (CBC) stem cells and +4 position cells in isolated colonic epithelial cells were detected. As shown in Fig. 3D, the mRNA levels of CBC stem cell markers *Lgr5*, *Axin2*, *Ascl2*, *Ephb3*, and *Ephb2* in WT colitis mice were significantly down-regulated, which were reversed by SNX10 deficiency. However, the mRNA expression of +4 position cell markers *Bmi1*, *Hopx*, *Lrig1*, and *Tert* did not show meaningful and concordant changes (fig. S3F). Although the reduction of ISC marker genes in the TNBS model was not significant, SNX10 deficiency up-regulated *Lgr5*, *Axin2*, and *Ascl2* mRNA levels (fig. S3G). These data suggest that SNX10 mainly is involved in CBC stem cells but not +4 position cell maintenance. To confirm it, IECs isolated from the ileum or colon were used for organoid in vitro culture. Consistent with increased regeneration in vivo,

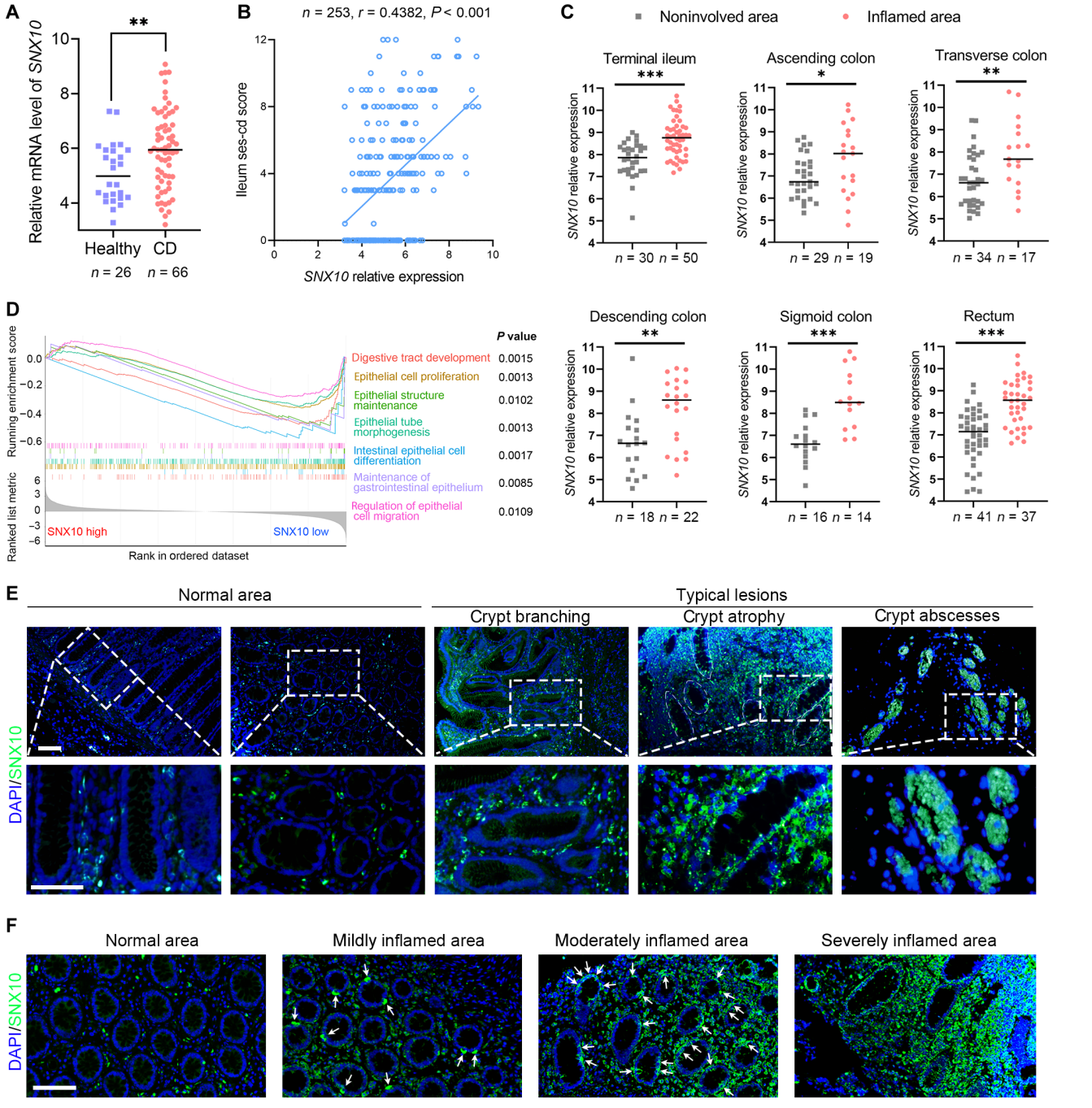

Fig. 1. SNX10 expression in intestinal tissues positively correlates with the severity of IBD. (**A**) *SNX10* mRNA expression in health controls ($n = 26$) and active patients with CD ($n = 66$) of the GSE112366 dataset. (**B**) The correlation between *SNX10* mRNA expression in biopsy samples and ileum simple endoscopic score for CD (ses-cd) from GSE112366 was analyzed by Spearman ($n = 253$). (**C**) *SNX10* mRNA expression in inflamed and noninvolved areas of different intestinal segments from the GSE100833 dataset. (**D**) Patients with CD were divided into the high *SNX10* expression group and the low *SNX10* expression group according to the median of *SNX10* mRNA level in the biopsy samples (GSE100833, $n = 1717$). Gene set enrichment analysis (GSEA) of indicated gene sets in CD patients with SNX10 low expression versus SNX10 high expression was conducted. In one analysis, a nominal *P* value was shown. (**E**) Immunofluorescent staining of SNX10 in normal or typical lesion areas of the colon from patients with CD. All scale bar, 50 μm. (**F**) Immunofluorescent staining of SNX10 in the areas of varying degrees of inflammation of colon tissues from patients with CD. White arrows indicate SNX10-positive epithelial cells. Scale bar, 100 μm. Data are represented as means ± SD. $^*P < 0.05$, $^{**}P < 0.01$, and $^{***}P < 0.001$. DAPI, 4′,6-diamidino-2-phenylindole.

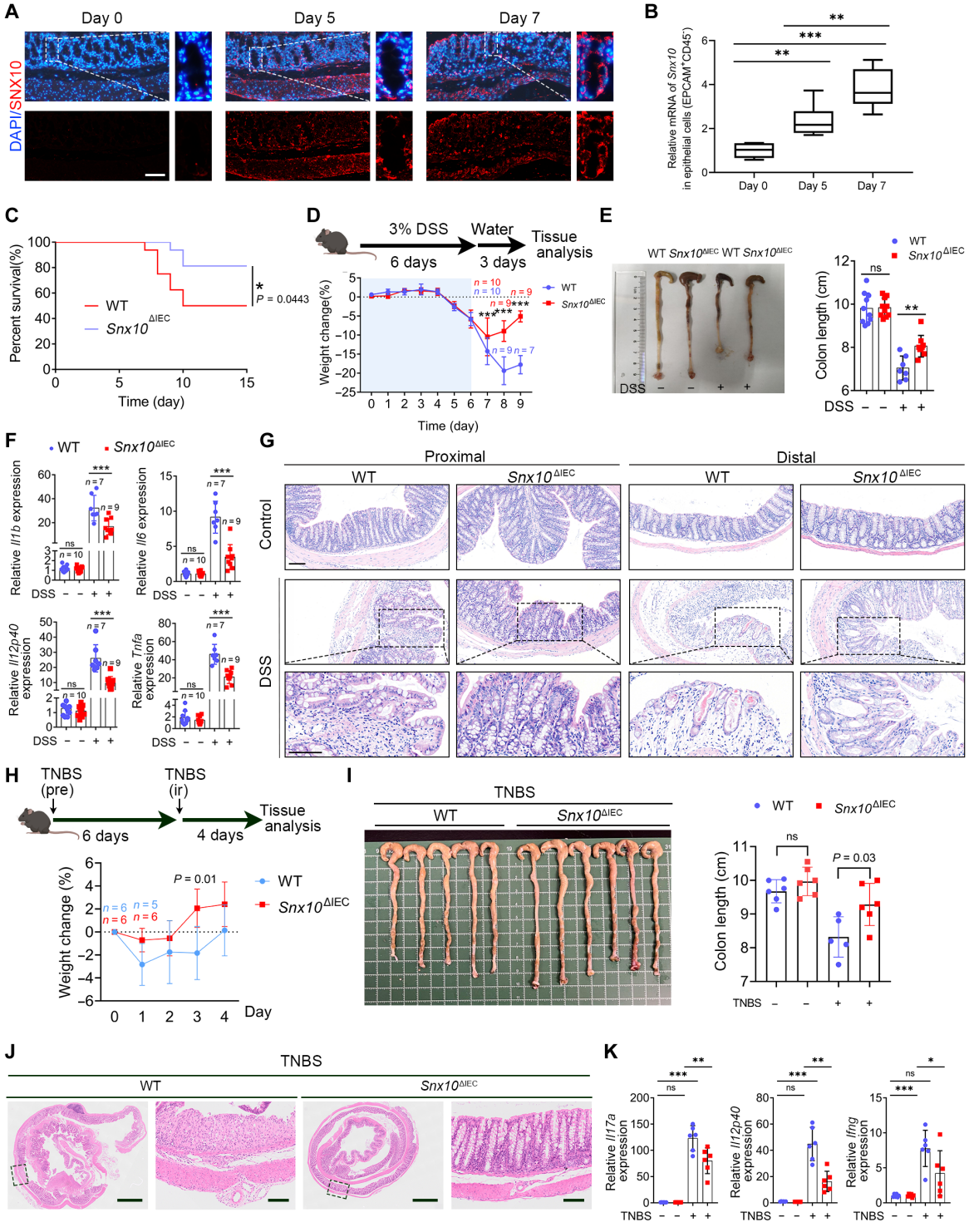

Fig. 2. Intestinal epithelium SNX10 deletion alleviated DSS-induced colitis and mucosal injury. (**A**) Immunofluorescent staining of SNX10 in colon sections of DSS-treated mice. Scale bar, 50 μm. (**B**) Relative mRNA levels of *Snx10* in colonic epithelial cells (EPCAM^{+}CD45^{-}) isolated from DSS-treated mice ($n = 6$). (**C**) Survival curve of *Snx10*$^{fl/fl}$ (WT) and *Snx10*$^{fl/fl}$;*Vil-Cre*$^{+}$ (*Snx10*$^{\Delta IEC}$) mice ($n = 16$) subjected to colitis induction with 3% DSS for 6 days, followed by regular drinking water. (**D**) Body weight change of mice treated with 3% DSS for 6 days, followed by regular drinking water for 3 days ($n = 10$). (**E**) The colon length of WT and *Snx10*$^{\Delta IEC}$ mice treated with DSS on day 9. (**F**) Relative mRNA levels of proinflammatory cytokines in the colon tissue measured by reverse transcription quantitative polymerase chain reaction (RT-qPCR) ($n =$ 7 to 10). (**G**) Representative hematoxylin and eosin (H&E) staining images of WT and *Snx10*$^{\Delta IEC}$ mice on day 9. Scale bar, 100 μm. (**H**) Body weight change of mice ($n = 6$) treated with 1% (w/v) TNBS presensitization solution for 6 days, followed by 2.5% (w/v) TNBS intrarectal (ir) delivery (at day 0). (**I**) The colon length of WT and *Snx10*$^{\Delta IEC}$ mice induced with TNBS on day 4. (**J**) Representative H&E staining images of WT and *Snx10*$^{\Delta IEC}$ mice treated with TNBS. Scale bars, 100 μm. (**K**) Relative mRNA levels of proinflammatory cytokines in the colon tissue measured by RT-qPCR ($n = 6$). Data are represented as means ± SD. ns, not significant *$P < 0.05$, **$P < 0.01$, and ***$P < 0.001$.

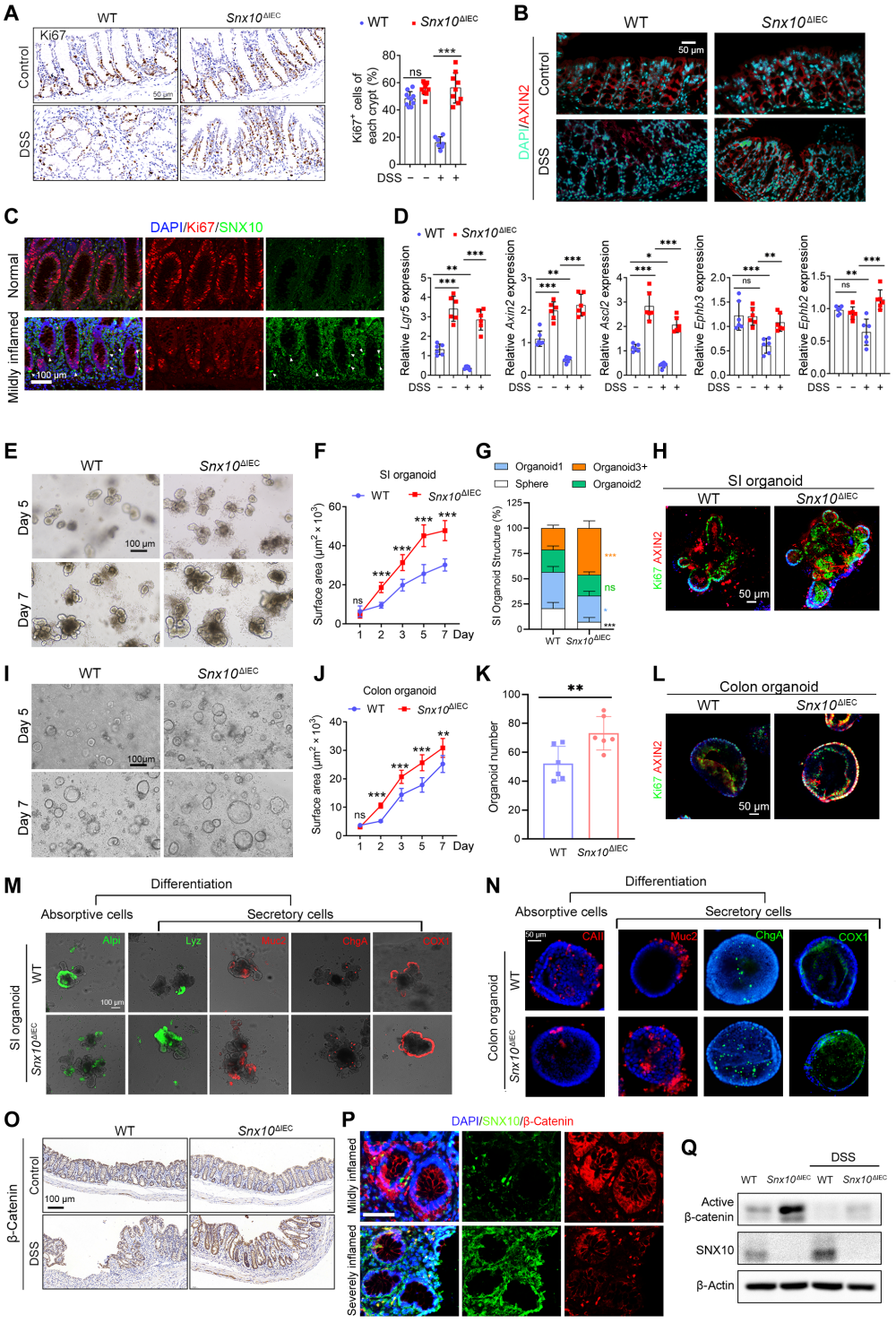

Fig. 3. SNX10 deficiency enhanced the stemness of CBC stem cells and promoted the differentiation of secretory-lineage cells. (**A**) Representative immunohistochemistry (IHC) images of Ki67 in colon sections and positive cell count in each crypt. (**B**) Immunofluorescent staining of AXIN2 in colon sections. (**C**) Immunofluorescent staining of Ki67 and SNX10 in colon tissues from patients with CD. White arrows: SNX10-positive epithelial cells. (**D**) ISC signature gene expression in colonic epithelial cells isolated from colitis mice. (**E**) Small intestinal (SI) organoids cultured from WT or *Snx10*$^{\Delta IEC}$ mice. (**F**) Average surface area and (**G**) structure quantification (based on the number of buds) of SI organoids ($n = 5$, 30 organoids per mouse). (**H**) Immunofluorescent staining of Ki67 or AXIN2 in SI organoids on day 7. (**I**) Representative images of colon organoids. (**J**) Average surface area and (**K**) quantification of colon organoids ($n = 6$, 30 organoids per mouse). (**L**) Immunofluorescent staining of Ki67 or AXIN2 in colon organoids on day 7. (**M** and **N**) Immunofluorescent staining of differentiation markers (Alpi or CAII: absorptive cells, Lyz: Paneth cells, Muc2: goblet cells, ChgA: enteroendocrine cells, COX1: tuft cells) in organoids on day 5. (**O**) Representative IHC images of β-catenin in the colon sections. (**P**) Immunofluorescent staining of β-catenin and SNX10 in the areas with different degrees of inflammation of colon tissues from patients with CD. Scale bar, 100 μm. (**Q**) Immunoblots for active β-catenin in colonic epithelial cells isolated from colitis mice. Data are represented as means ± SD. *$P < 0.05$, **$P < 0.01$, and ***$P < 0.001$.

loss of SNX10 led to an elevation in size and complexity (higher number of buds) of small intestinal (SI) organoids (Fig. 3, E to G). Immunostaining of AXIN2 and Ki67 revealed that loss of SNX10 caused greater self-renew capacity of IECs in SI organoids (Fig. 3H). ISCs among dispersed colonic epithelial cells cultured by WENR medium [epidermal growth factor (EGF), Noggin and R-spodin-1 containing (ENR) medium plus 10% Wnt3a-conditioned medium] developed into spherical organoids without buds. We also observed an increase in the size and number of colon organoids developed from *Snx10*$^{\Delta IEC}$ ISCs (Fig. 3, I to K), indicating a greater expansion capacity in vitro. This was further confirmed by AXIN2 and Ki67 staining (Fig. 3L). Immunofluorescent staining of the markers for

lineage differentiation (Alpi for enterocytes, Lyz for Paneth cells, Muc2 for goblet cells, ChgA for enteroendocrine cells, COX1 for tuft cells, and CAII for colonocytes) revealed that *Snx10* deficiency resulted in a shift to the secretory lineage in both SI and colon organoids (Fig. 3, M and N), consistent with the results from DSS-induced mice. The activation of the Wnt pathway was reported to promote the differentiation of secretory epithelial cells (*30*). Consistently, we also observed that SNX10 deficiency caused a significant increase of β-catenin in the epithelium of colitis mice and organoids (Fig. 3O and fig. S3, H and I). Similarly, SNX10 expression in the crypt of patients with CD was negatively correlated with β-catenin expression (Fig. 3P). WB analysis also revealed active (nonphosphorylated at $Ser^{33/37}/Thr^{41}$) β-catenin increased in isolated $EPCAM^+CD45^-$ epithelial cells from $Snx10^{\Delta IEC}$ colitis mice (Fig. 3Q and fig. S3J) supporting an activated Wnt signaling pathway by SNX10 deficiency. Collectively, our data suggest that $Snx10^{\Delta IEC}$ promoted mucosal repair through up-regulation of Wnt-driven ISC regeneration.

Lgr5-ISC–specific SNX10 deficiency maintained the ISC pool to accelerate the intestinal epithelial repair

$LGR5^+$ CBC cells as the main ISC population are responsible for self-renew of IECs. It has been reported that the canonical colonic stem cell signature is disrupted in CD (*6*). As expected, GSE100833 dataset analysis revealed that *LGR5* expression was significantly decreased in patients with CD compared with healthy controls and positively correlated with disease severity (fig. S4, A and B). Consistent with the CBC stem cell signature gene expression in mice (Fig. 3C), the transcriptome landscape of guts in CD patients with low SNX10 expression presented a positive stem cell–associated signature (Fig. 4A). In addition, the $LGR5^+$ ISC signature genes, which were up-regulated in $Snx10^{\Delta IEC}$ mice, were negatively correlated with SNX10 expression in patients with CD (Fig. 4B). These data imply a tight bond between SNX10 expression and stem cell fate. SNX10 has been listed as one of 384 signature genes of CBC stem cells by analyzing the transcriptional profiles of fluorescence-activated cell sorting–sorted $LGR5^+$ cells in an earlier study (*31*). To further confirm that CBC stem cells were the main ISCs affected by SNX10 deficiency, *Lgr5-EGFP-IRES-CreERT2* mice were introduced for direct labeling of CBC stem cells. As shown in Fig. 4C, $LGR5^+$ cells in the crypt base coexpressed SNX10 on day 5 after DSS induction. Consistent with the clinical data on regenerative capacity, we observed an elevated staining of SNX10 in the crypts of severely inflamed areas accompanied by a decrease in the number of CBC stem cells ($OLFM4^+$) (Fig. 4D). To delete SNX10 in the ISCs, *Lgr5-EGFP-IRES-CreERT2*;$Snx10^{fl/fl}$ mice were generated and induced by tamoxifen. As expected, Lgr5-ISC–specific SNX10 deficiency ($Snx10^{\Delta ISC}$) significantly reduced the mortality (fig. S4C), promoted weight recovery (Fig. 4E), and ameliorated colon shortening (Fig. 4F) in DSS-induced colitis mice. Fluorescence imaging revealed that there were more crypts containing $LGR5^+$ cells in the colon of $Snx10^{\Delta ISC}$ mice during recovery (on day 9; Fig. 4, G and H). Notably, more $LGR5^+$ ISC–containing crypts could be found at the inflammatory cell infiltrated areas in the colon of $Snx10^{\Delta ISC}$ mice before recovery (on day 6; Fig. 4I), suggesting that SNX10 deficiency–induced ISC expansion occurred in the inflammation phase, despite the differences in epithelial structure and body weight between WT and $Snx10^{\Delta ISC}$ mice that could only be found in the repair phase. Consistent with pathological changes in vivo, Lgr5-ISC–specific SNX10 deficiency increased the number of $LGR5^+$ cells and the growth efficiency of SI and colon organoids (Fig. 4, J and K, and fig. S4, D and E). These results suggest that SNX10 acts as a suppressor in regulating the stemness of ISCs in the inflammatory environment, and targeted inhibition of SNX10 might be a promising strategy for restoring intestinal mucosa barrier function.

The increased cholesterol biosynthesis by SNX10 deletion contributed to intestinal epithelial repair

To determine the mechanism by which SNX10 restricted ISC amplification, we compared the transcriptome of isolated epithelial cells from WT and $Snx10^{\Delta IEC}$ colitis mice. As shown in Fig. 5A, the isoprenoid metabolic process genes were enriched in epithelial cells from $Snx10^{\Delta IEC}$ mice. Similarly, in biopsy samples from inflamed areas of patients with CD, cholesterol biosynthesis genes enriched in the low SNX10 group (fig. S5A). Several previous genetic studies reported that the *SNX10* gene is a signature locus in altering lipid metabolism (*19*–*23*). Further clinical data analysis revealed that SNX10 expression presented a weak negative correlation ($0.2 < r < 0.4$) with fatty acid biosynthesis genes and moderate or strong negative correlation ($0.4 < r < 0.8$) with cholesterol biosynthesis genes (fig. S5, B and C), suggesting that SNX10 was involved in the biosynthesis of lipids, especially cholesterol in colitis. Considering that cholesterol availability is necessary for the self-renewal of ISCs (*9*), we hypothesized that the restriction of ISC regeneration caused by SNX10 up-regulation in the inflammatory intestine was due to the altered cholesterol biosynthesis. To understand the involvement of SNX10 in ISC renewal and cholesterol synthesis, we arranged the ISC signature genes and the cholesterol synthesis genes according to the value of correlation coefficient (r) with SNX10 and plotted a matrix to show the correlation between the ISC renewal genes and cholesterol synthesis genes. As shown in Fig. 5B, the blue area converging in the lower right corner of the heatmap indicates coexpression relationships between the corresponding ISC renewal genes and cholesterol synthesis genes. These coexpressed genes also have strong negative correlations with SNX10 expression, indicating a potential link role of SNX10 in ISC renewal and cholesterol synthesis. Immunostaining revealed a strong negative correlation between the number of $SNX10^+$ cells and the number of $HMGCR^+$ cells per crypt in the inflamed area of patients with CD (Fig. 5C and fig. S5D). Next, we enquired whether this correlation could be verified in a DSS-induced colitis model. Cholesterol measurement and filipin staining showed that SNX10 deficiency enhanced cholesterol levels in the colons of colitis mice (Fig. 5D and fig. S5E). Consistent with clinical data, the expression of 3-hydroxy-3-methylglutaryl-CoA reductase (HMGCR), a rate-limiting enzyme in cholesterol synthesis, was significantly up-regulated by SNX10 deficiency (Fig. 5E). Methyl-β-cyclodextrin (MβCD) was used to eliminate the difference in the cholesterol content between WT and SNX10-deficient organoids. Within 16 hours after MβCD treatment, SNX10 deficiency significantly accelerated cholesterol synthesis in SI and colon organoids (Fig. 5, F and G). Lovastatin (5 μM), an enzyme activity inhibitor of HMGCR, could abolish the increase of cholesterol content, SI organoid budding, and colonic organoid colony caused by SNX10 deficiency (Fig. 5, H and I, and fig. S5, F and G). However, the expression of cholesterol synthesis and fatty acid synthase genes was significantly up-regulated in SNX10-deficient organoids with or without lovastatin (Fig. 5J and fig. S5H). Consistent with the result of organoid development, lovastatin erased the $SNX10^{\Delta IEC}$-induced up-regulation of ISC gene expression, which could be rescued by mevalonic acid (fig. S5I).

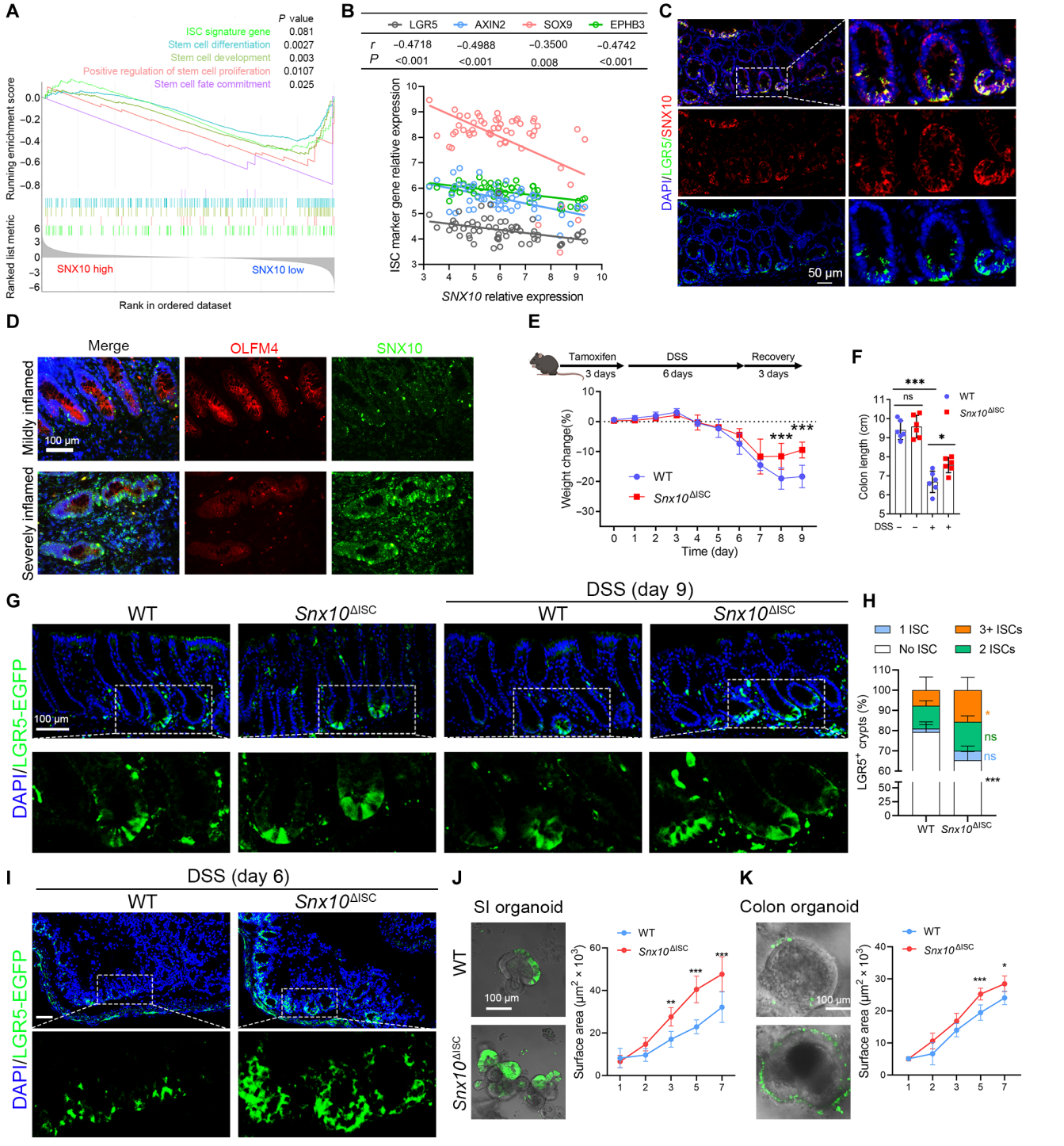

Fig. 4. Lgr5-ISC–specific SNX10 deficiency retained the ISC pool for accelerating the epithelial repair. (**A**) GSEA of indicated gene sets in CD patients with SNX10 low expression versus SNX10 high expression from GSE100833 ($n = 1717$). (**B**) Correlation analysis by Spearman between *SNX10* and ISC marker gene expression in CD patients with moderate or severe endoscopic activity from GSE112366 ($n = 56$). (**C**) Immunofluorescent staining of SNX10 and LGR5-EGFP (enhanced green fluorescent protein) in colon sections from colitis mice. (**D**) Immunofluorescent staining of OLFM4 and SNX10 in inflamed colon tissues from patients with CD. (**E**) Body weight change of WT and *Snx10*$^{\Delta ISC}$ mice ($n = 6$, tamoxifen-induced) subjected to colitis induction with 3% DSS for 6 days, followed by regular drinking water. (**F**) Colon length of WT and *Snx10*$^{\Delta ISC}$ mice on day 9. (**G**) Histology of the recovery region in the colon from WT or *Snx10*$^{\Delta ISC}$ mice on day 9. (**H**) Quantification of crypts with 0, 1, 2, or 3+ EGFP^{+} cells in recovery region (~50 crypts per mouse, six mice per group). (**I**) Histology of the inflamed region in the colon from WT or *Snx10* $^{\Delta ISC}$ DSS-induced mice (day 6). Scale bar, 100 μm. (**J**) Images of SI organoids and (**K**) colon organoids on day 5 from WT or *Snx10*$^{\Delta ISC}$ mice (left). The average surface area of 30 organoids per mouse ($n = 5$) was measured (right). Data are represented as means ± SD. *$P < 0.05$, **$P < 0.01$, and ***$P < 0.001$.

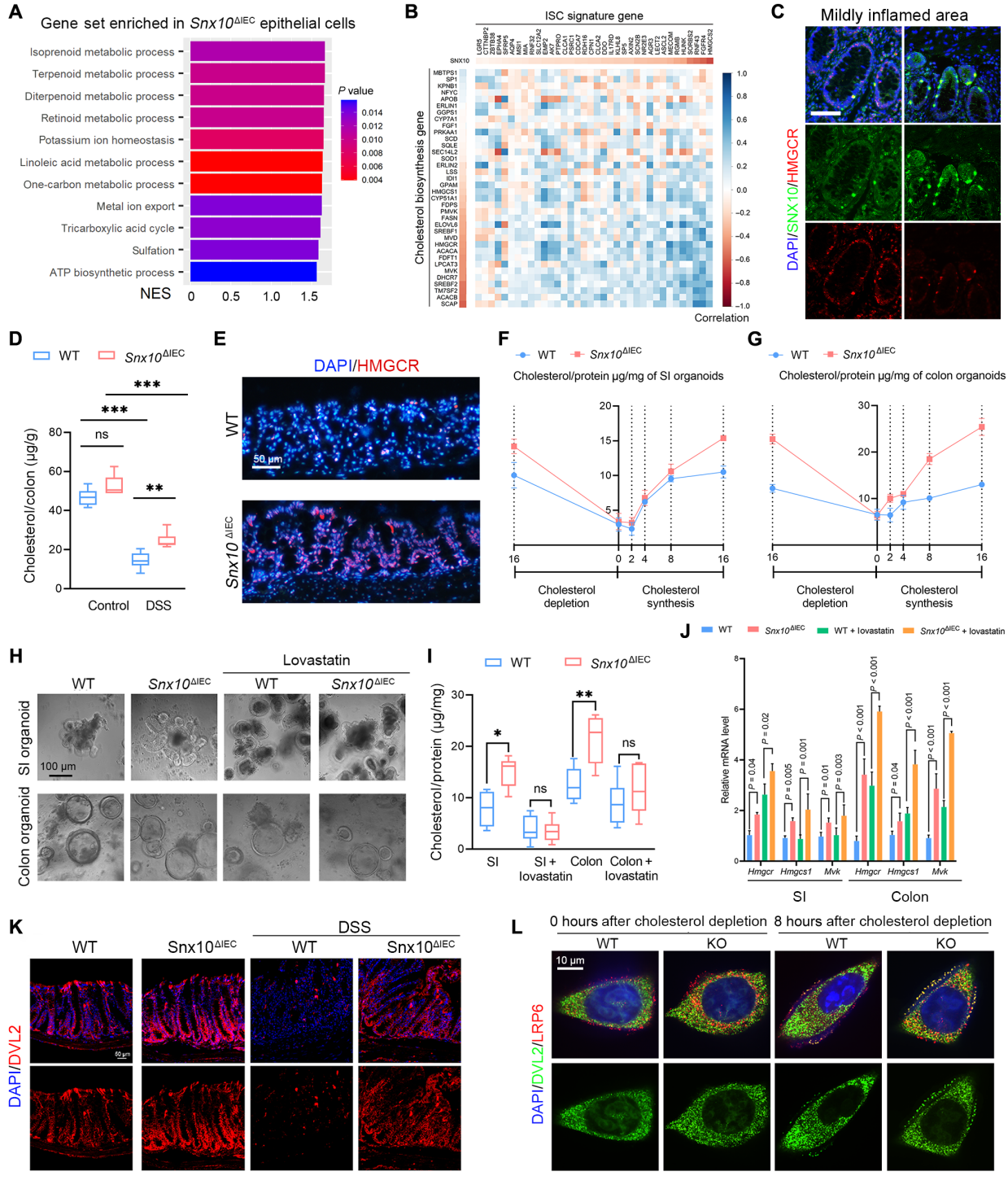

Fig. 5. The increased cholesterol biosynthesis by SNX10 deletion contributed to intestinal epithelial repair. (**A**) GSEA of gene sets enriched in colonic epithelial cells from *Snx10*$^{\Delta IEC}$ mice (versus WT mice) with DSS colitis ($n = 3$). (**B**) Correlation analysis (by Spearman) matrix between ISC signature genes and cholesterol biosynthesis genes in the inflamed area from patients with CD of GSE100833 ($n = 369$). (**C**) Immunofluorescent staining of 3-hydroxy-3-methylglutaryl-CoA reductase (HMGCR) and SNX10 in inflamed areas of colon tissues from patients with CD. Scale bar, 100 μm. (**D**) Free cholesterol content in colonic epithelial cells isolated from colitis mice ($n = 6$). (**E**) Immunofluorescent staining of HMGCR in colon sections. (**F**) SI and (**G**) colon organoids were treated with 500 μM methyl-β-cyclodextrin (MβCD) for 16 hours, and then replaced with normal medium for 16 hours. Free cholesterol content at different times was measured. (**H**) Representative images of organoids treated with or without lovastatin (5 μM) on day 6. (**I**) Free cholesterol content of organoids ($n = 5$). (**J**) Relative mRNA levels of cholesterol biosynthesis gene in organoids ($n = 3$). (**K**) Immunofluorescent staining of Dishevelled2 (DVL2) in colon sections from DSS-treated mice. Scale bar, 50 μm. (**L**) Immunofluorescent staining of DVL2 and LRP6 in HCT116 cells that were treated with serum-free medium containing 500 μM MβCD for 16 hours, and then replaced with serum-free medium for 8 hours, followed by additional Wnt3a (200 ng/ml) for another 2 hours. Data are represented as means ± SD. *$P < 0.05$, **$P < 0.01$, and ***$P < 0.001$. NES, normalized enrichment score.

These data suggest that mevalonic acid supplementation directly skipped the inhibition of lovastatin on HMGCR and rescued the phenotype. In addition, we evaluated the effect of lovastatin on intestinal cholesterol levels and intestinal inflammation in the absence or presence of SNX10 during colitis. As shown in fig. S5 (J to L), although lovastatin and SNX10 epithelial KO alleviated weight loss, they had opposite effects on cholesterol levels in epithelial cells, demonstrating that the ameliorative effect of lovastatin on colitis is not dependent on cholesterol synthesis. In *Snx10*$^{\Delta IEC}$ mice, lovastatin lowered cholesterol levels and impaired the ameliorative effect of SNX10 deletion in the recovery phase. This can be explained by the strong inhibitory activity of lovastatin that overrides the *Snx10*$^{\Delta IEC}$-induced increase of HMGCR expression, ultimately leading to the decreased cholesterol level and attenuated *Snx10*$^{\Delta IEC}$ phenotype in colitis. Previous studies suggest that cholesterol selectively activates the canonical Wnt pathway by specifically facilitating the membrane recruitment of Dishevelled2 (DVL2) (*32*). We then further examined whether the increased cholesterol by SNX10 deficiency was associated with DVL2-mediated Wnt pathway activation. Immunofluorescence showed that SNX10 deficiency significantly increased DVL2 staining in the colonic epithelial cells of mice with colitis (Fig. 5K). In vitro experiments showed that cholesterol depletion abolished the colocalization of DVL2 with LRP6 on the plasma membrane, while cholesterol synthesis resulted in a stronger colocalization of DVL2 and LRP6 in SNX10-deficient cells, suggesting that the enhanced Wnt pathway activation by SNX10 deficiency is due to the increased cholesterol synthesis (Fig. 5L). Collectively, these data demonstrate that SNX10 deficiency increased cholesterol synthesis and thus promoted epithelial repair.

Disassociation of ERLIN2 with SCAP induced by SNX10 deletion enhanced SREBP2 activation contributing to the increased cholesterol biosynthesis

SREBPs are the main regulators of cholesterol metabolism. To explore the mechanism underlying the increased cholesterol biosynthesis caused by SNX10 deletion, we first ruled out the possibility that SNX10 deletion might increase the transcript levels of SREBP1 or SRBEP2 in both SI and colon organoids (fig. S6A). The activation of SREBPs is mainly regulated by the cleavage of their precursor. By WB, we observed a marked increase of cleavage products (N terminus) and a decrease of SREBP1 and SREBP2 precursors in SI and colon organoids from *Snx10*$^{\Delta IEC}$ mice. Notably, it was SREBP2, but not SREBP1, that still showed an increased N terminus in colon organoids with lovastatin treatment (Fig. 6A), suggesting that SRBEP2 cleavage might be directly altered by SNX10 deletion. Hence, we further investigated the mechanism by which SNX10 regulates SREBP2 cleavage. We first confirmed that SNX10 KO by CRISPR significantly increased the nuclear localization of SREBP2 (Fig. 6B). As reported, upon sensing a low level of cellular cholesterol, pre-SRBEP2 is transported from the ER to the Golgi apparatus for cleavage into a nuclear-localized mature form (*33*). As shown in Fig. 6C and fig. S6B, both nuclear and Golgi translocation of SREBP2 were largely enhanced by SNX10 KO under control or cholesterol treatment. Impressively, these results were reversed by SNX10 rescue (fig. S6, C and D). Live cell imaging showed that mCherry-tagged SNX10 localized at ER instead of the Golgi apparatus regardless of additional cholesterol (fig. S6E). On the basis of the above findings, we assumed that SNX10 might be involved in the anchoring of SREBP2 on the ER and thereby limited its Golgi transport. When the cellular cholesterol level reaches a certain threshold, the SREBP2-SCAP-INSIG-ERLIN2 complex is anchored to the ER membrane, and therefore, SREBP2-SCAP is unable to translocate to the Golgi apparatus (*33*, *34*). We virtually docked the structures of SNX10 (4PZG) (*35*) and SCAP in the presence of 25-hydroxycholesterol (6M49) (*36*). The predicted interfaces are based on residues 153 to 155 of SNX10, which are important for their binding to proteins (*37*) and can be blocked by a PPI inhibitor DC-SX029 (*17*). If we blocked these residues, then the predicted interaction between SCAP and SNX10 was greatly reduced (fig. S6F). Consistent with the docking results, SREBP2 precursor, ERLIN2, and SCAP were pulled down by Flag-tagged SNX10, and these interactions were attenuated in DC-SX029–treated cells (Fig. 6D). Meanwhile, SREBP1 was not pulled down by SNX10-Flag (Fig. 6D). Notably, SNX10 KO significantly inhibited the pull-down of SCAP by endogenous ERLIN2 (Fig. 6E), and SNX10 reintroduction rescued the interaction between ERLIN2 and SCAP (fig. S6G). Immunofluorescence staining displayed the colocalization of SNX10 with ERLIN2 or SCAP being significantly enhanced by additional cholesterol, further confirming a function of SNX10 in anchoring SREBP2-SCAP to ER through interacting with ERLIN2 (Fig. 6, F and G, and fig. S6, H and I). These data suggest that the disassociation of ERLIN2 with SCAP by SNX10 deletion is responsible for SREBP2 activation and thereby promotes cholesterol biosynthesis.

SNX10 PPI DC-SX029 promoted epithelial repair by enhancing the SREBP2-mediated stemness of ISCs

Next, we investigated the feasibility of targeting SNX10 to promote intestinal epithelial repair in IBD. WB analysis showed that DC-SX029 significantly facilitated the cleavages of SREBP2 in SI and colon organoids (Fig. 7A). As expected, free cholesterol content was increased in DC-SX029–treated SI and colon organoids (Fig. 7B). RT-qPCR analysis showed that DC-SX029 promoted the transcription of ISC signature genes and cholesterol biosynthesis (Fig. 7, C and D). Accordingly, the size and regeneration capacity of the SI and colon organoids were significantly elevated (Fig. 7, E and F). Oral administration of DC-SX029 has been reported to be effectively ameliorated DSS-induced colitis in our previous studies (*17*). Here, we examined the effect of DC-SX029 on the regeneration capacity of epithelial cells in colitis mice. Immunohistochemistry (IHC) staining showed that DC-SX029 significantly increased the number of crypts where Ki67 and β-catenin were highly expressed (Fig. 7G). Cholesterol measurement showed that DC-SX029 enhanced the cholesterol level in the colons of colitis mice (Fig. 7H). The expression of ISC signature gene *Lgr5*, *Axin2*, and *Ascl2* in isolated epithelial cells was increased in the DC-SX029 group (Fig. 7I). Consistently, oral administration of DC-SX029 significantly elevated the number of LGR5-EGFP (enhanced green fluorescent protein) cells, showing better efficacy than mesalazine at a dose of 50 mg/kg per day in vivo (Fig. 7J). Rescue experiments showed that DC-SX029 treatment after the onset of symptoms still promoted weight restoration and alleviated colon shortening, inflammatory cell infiltration, and crypt loss of both DSS-induced and TNBS-induced colitis mice (figs. S7, A to C, and S8, A to C). Consistently, DC-SX029 effectively reduced pro-inflammatory cytokines and increased ISC marker gene expression (figs. S7, D and E, and S8, D and E). Compared to mesalazine, DC-SX029 was superior in promoting ISC regeneration and suppressing IL12p40 expression. Ki67 and β-catenin staining results also indicated that DC-SX029 enhanced ISC-mediated intestinal epithelial regeneration in colitis mice (figs. S7, F and G, and S8, F

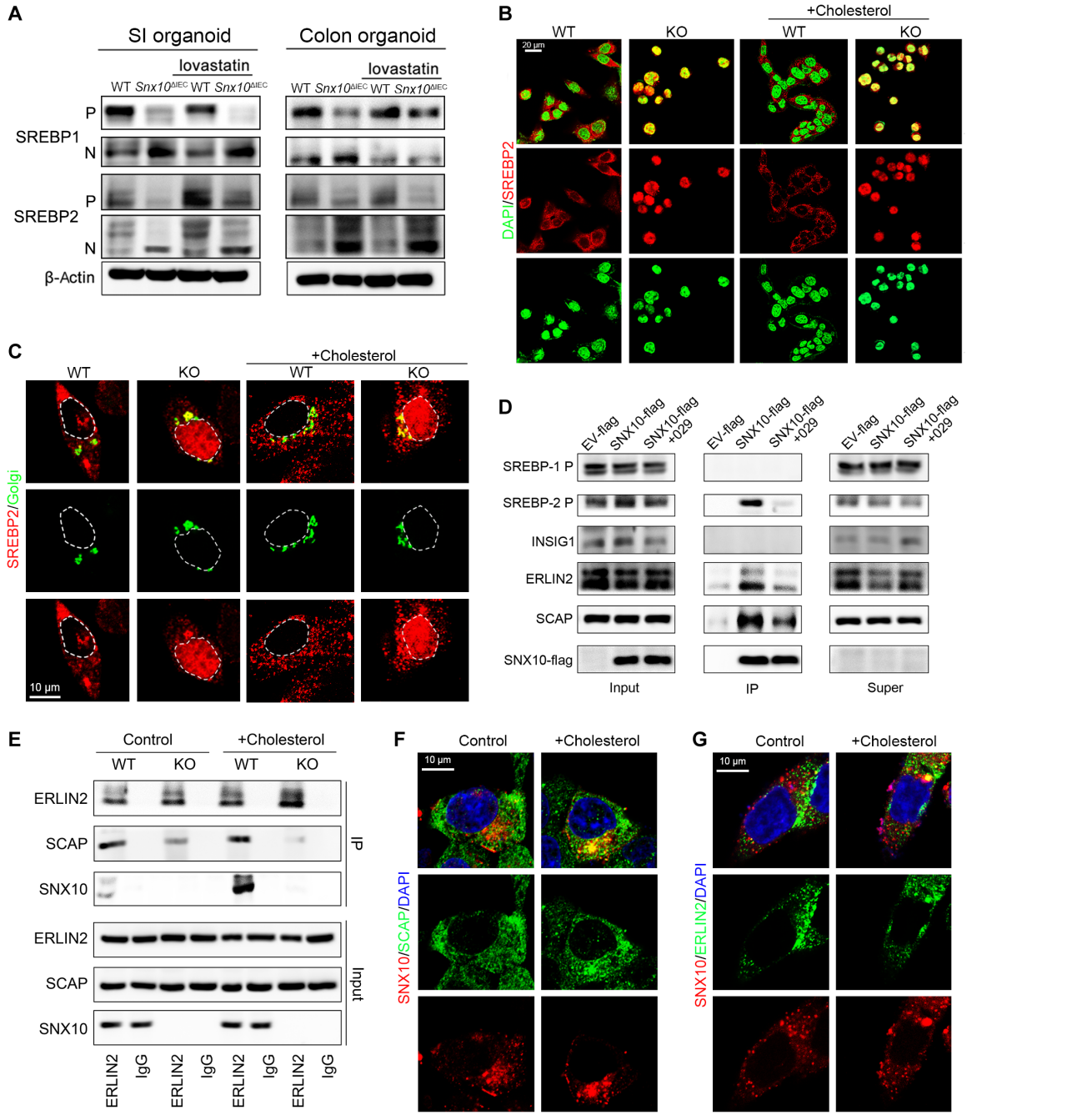

Fig. 6. Disassociation of ERLIN2 with SCAP induced by SNX10 deletion enhanced SREBP2 activation contributing to the increased cholesterol biosynthesis. (**A**) Representative immunoblots for precursors (P) and N-terminal cleavage fragments (N) of SREBP1 and SREBP2 in SI or colon organoids with or without lovastatin from WT or *Snx10*$^{\Delta IEC}$ mice. (**B**) Immunofluorescent staining of SREBP2 in WT or SNX10 KO HCT116 cells with or without cholesterol (10 μg/ml) treatment for 12 hours in low-glucose Dulbecco's modified Eagle's medium (DMEM). (**C**) WT or SNX10 KO HCT116 cells 36 hours after transfected with CellLight Golgi-GFP were cultured with low-glucose DMEM in the presence or absence of cholesterol (10 μg/ml) for 12 hours, followed by immunofluorescent staining of SREBP2. (**D**) Lysates of HCT116 cells transfected with empty vector (EV)-*flag* or *SNX10-flag* plasmids were prepared and subjected to immunoprecipitation with anti-FLAG M2 agarose beads, followed by a WB with the indicated antibodies. (**E**) Lysates of WT or KO HCT116 cells without or with cholesterol treatment for 12 hours were subjected to immunoprecipitation with anti-ERLIN2 antibody, followed by a WB with the indicated antibodies. (**F** and **G**) Immunofluorescent staining of SNX10 and SCAP or ERLIN2 in HCT116 cells without or with cholesterol treatment for 12 hours. IgG, immunoglobulin G.

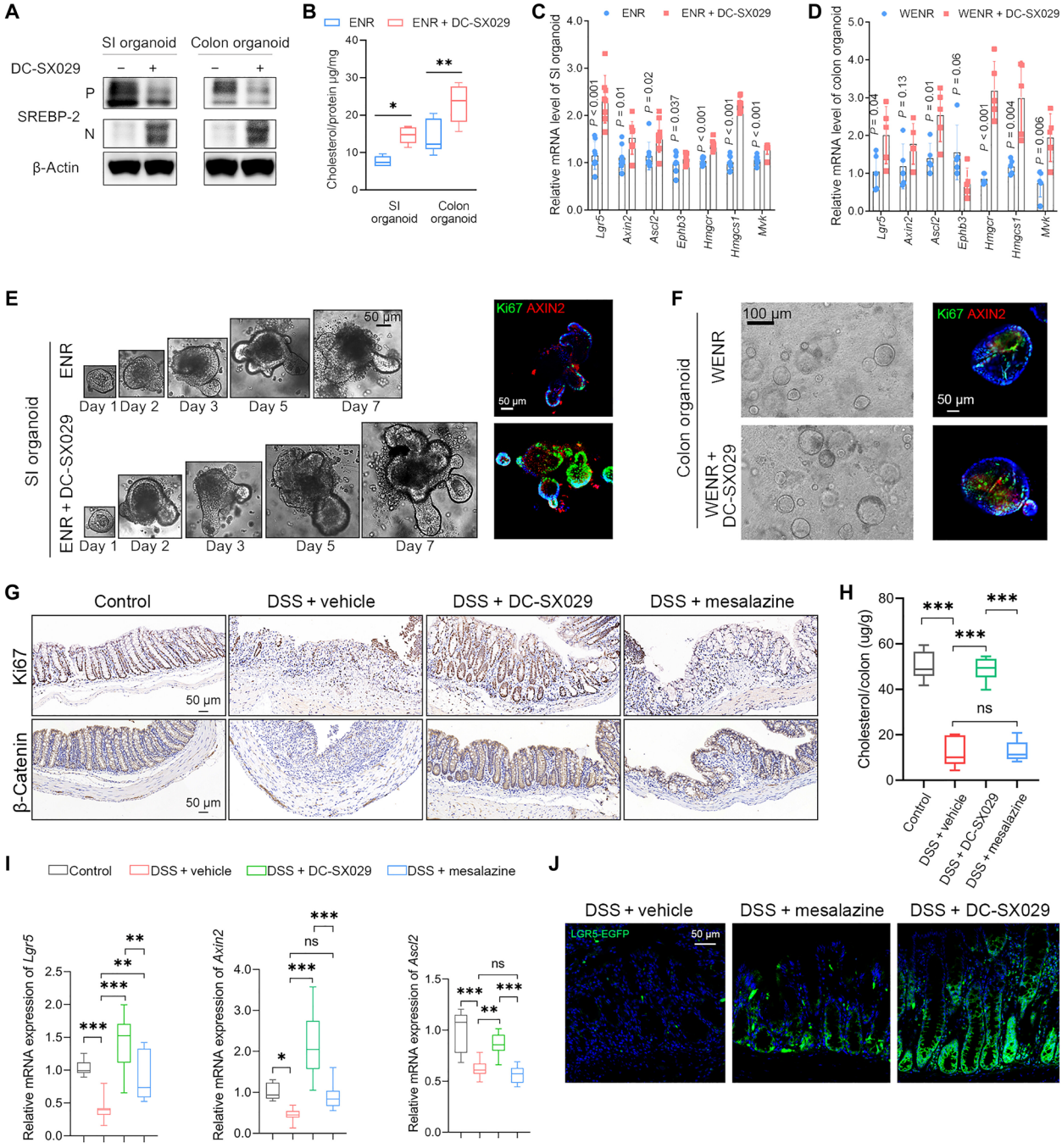

Fig. 7. SNX10 PPI DC-SX029 promoted epithelial repair by enhancing the SREBP2-mediated stemness of ISCs. (**A**) Representative immunoblots for SREBP2 in SI or colon organoids with or without DC-SX029 (50 μM) treatment for 7 days. (**B**) Free cholesterol content in SI or colon organoids with or without DC-SX029 treatment for 7 days. (**C** and **D**) Relative mRNA levels of ISC signature genes and cholesterol biosynthesis genes in SI or colon organoids measured by RT-qPCR. (**E**) SI organoids were cultured in ENR medium without or with DC-SX029 (50 μM) for 7 days, followed by immunostaining with the antibodies against Ki67 and Axin2. (**F**) Colon organoids were cultured in WENR medium without or with DC-SX029 (50 μM) for 7 days, followed by immunostaining with the antibodies against Ki67 and Axin2. (**G**) Representative IHC images of Ki-67 and β-catenin in colon sections from each group on day 9. Scale bars, 50 μm. Mice ($n = 10$) were treated with 3% DSS for 6 days, followed by regular drinking water for 3 days. Mesalazine (50 mg/kg per day) or DC-SX029 (2 mg/kg per day) was given intragastrically during the whole process. (**H**) Free cholesterol content in colonic epithelial cells isolated from the indicated groups ($n = 6$). (**I**) Relative mRNA levels of ISC signature genes in colon epithelial cells isolated from the indicated groups measured by RT-qPCR ($n = 10$). (**J**) Immunofluorescent images of colon sections from *Lgr5-EGFP* mice in each group. Scale bar, 50 μm. Data are represented as means ± SD. Data of Fig. 6 (B to D) were compared by two-sided unpaired *t* test. Data of Fig. 6H were compared by one-way analysis of variance (ANOVA) followed by the Bonferroni post hoc test. $^*P < 0.05$, $^{**}P < 0.01$, and $^{***}P < 0.001$.

and G). Collectively, DC-SX029 as an SNX10 PPI, effectively relieved mouse colitis by promoting SREBP2-mediated intestinal epithelial repair.

DISCUSSION

Clinical studies have shown that the number of $LGR5^+$ ISCs in the intestinal epithelium of patients with CD (*6*) is significantly lower than in patients with ulcerative colitis (*38*, *39*). Similarly, $LGR5^+$ ISCs were nearly depleted in the DSS-induced model (*40*). Several studies based on this model have confirmed the importance of $LGR5^+$ ISCs in intestinal epithelium repair (*41*, *42*). Therefore, the DSS-induced colitis mouse model was mainly used in the present study. Microarray analysis from a previous study indicated that SNX10 may be involved in the maintenance of ISCs (*31*). Here, we explored the function of SNX10 in maintaining the stemness of $LGR5^+$ ISCs and the potential to restore intestinal epithelial barrier function by in vitro organoid culture and in vivo two types of conditional KO mice, combined with analysis of clinical data. Our data suggest that SNX10 is an ISC signature gene but acts as an intrinsic limiter. Previously, it was reported that although SNX10 mRNA is highly expressed in ISCs under physiological conditions, the protein level of SNX10 in ISCs is not different from that in other IECs (*31*). This is consistent with our data that SNX10 protein was not expressed at the base of the crypt before chemical induction. In an inflammatory environment, both mRNA and protein levels of SNX10 in ISCs are significantly increased, which could result in the suppression of ISC function. Conversely, inhibition or deletion of SNX10 abolishes the restriction of ISC expansion via SREBP2–mediated cholesterol synthesis in colitis mice, suggesting a potentialnew strategy for CD treatment.

Secretory lineage differentiation favors mucosal repair in mouse (*43*) and human CD (*6*). In a homeostatic environment, the differentiation of ISCs is determined by the balance of Wnt and Notch signaling pathways (*30*). The Wnt pathway promotes the differentiation of ISCs toward the secretory lineage, whereas the Notch pathway promotes the absorptive lineage. In the present study, we confirm that the deletion of SNX10 activates the Wnt signaling pathway and shifts ISC differentiation toward the secretory cell lineage. This contributes to the beneficial effect of SNX10 deletion on the recovery of damaged epithelium of colitis mice. Different types of secretory cells derived from ISCs have distinct functions in mucosal repair. Goblet cells protect the damaged barrier from bacterial infection by secreting mucus (*44*). Tuft cells enhance prostaglandin E_2–mediated epithelial repair to mitigate chronic colitis in response to bacterial infection (*45*). Both goblet cells and tuft cells were significantly increased by SNX10 deficiency in mice with DSS-induced colitis, representing a pattern of cell lineage differentiation to facilitate mucosal repair. However, the increase in enteroendocrine cells by SNX10 deletion in organoids was not consistent with in vivo data, which might be, in part, due to the increased differentiation of secretory progenitor cells into enteroendocrine cells by DSS administration (*46*). A previous study accurately described the transient presence of fetal-like repair of epithelial cells characterized by increased Ki67 and reduced Muc2 expression in the DSS model (*47*). We found that SNX10 deficiency up-regulated not only Ki67 but also Muc2 in the crypt, suggesting a contribution of mucins to epithelial repair.

Cholesterol availability is critical for ISC stemness (*9*). Clinically, low plasma cholesterol has been recognized as a typical feature of patients with CD and correlated with disease severity (*10*–*12*, *48*–*50*). Apparently, low plasma cholesterol reduces the accessibility of cholesterol to ISCs, which could lead ISCs to rely on their own intracellular cholesterol biosynthesis. The ileum is the most frequently damaged region in the small intestine of CD. Accordingly, cholesterol biosynthesis was highly active in the ileal crypt compared with the other SI compartments (*51*). These findings inspired us to explore whether increased cholesterol biosynthesis in ISCs might be beneficial for the treatment of CD. Our study identifies SNX10 as a key gene that orchestrates cholesterol synthesis and ISC stemness. We observed that the increase in cholesterol synthesis caused by SNX10 deficiency enhanced the stemness of ISCs in both the small intestine and colon. In addition, the deletion of SNX10 also up-regulates key genes related to the fatty acid synthesis pathway, which are also important for the self-renewal of ISCs (*8*, *51*, *52*). Another interesting question raised is why statins reduce the risk of recurrence of CD (*53*, *54*) and alleviate inflammation in patients with CD (*55*). This seems to contradict our data showing that the increase in cholesterol content promotes ISC-mediated mucosal repair. The reported mechanisms underlying the relief of colitis by statins were not due to the inhibition of cholesterol biosynthesis but to fibroblast apoptosis (*56*), mucosal eNOS transcription (*57*), and the T_H1-polarized immune response (*58*). It can be speculated that the unfavorable effect of cholesterol-lowering by statins on intestinal epithelial repair might be overshadowed by other beneficial pharmacologic effects. Another concern is that increased cholesterol synthesis in immune cells may promote colitis. Cholesterol has been reported to activate the NACHT, LRR and PYD domains-containing protein 3 (NLRP3) inflammatory pathway in macrophages (*59*), thereby promoting caspase-mediated IL-1β release, which is an important driver for the development of intestinal inflammation in patients with CD (*60*, *61*). However, this concern can be excluded by our previous study, which demonstrated that loss of SNX10 in macrophages could significantly inhibit the inflammatory response induced by lipopolysaccharide or oxidation low-density lipoprotein (*17*, *18*, *23*). Collectively, SNX10 deficiency could promote mucosal healing by restoring the ISC stemness while inhibiting inflammation.

Cholesterol synthesis is mainly mediated by the nuclear factor SREBPs, which drive the transcription of key enzymes involved in this process. Activation of SREBPs requires cleavage in the Golgi before they function as transcription factors in the nucleus. Before cleavage, the precursors of SREBPs are anchored to ER by interacting with the ERLIN2-SCAP-INSIG1 complex (*34*). SCAP is a chaperone protein of SREBPs containing a sterol-sensing domain. Under cholesterol-sufficient conditions, the cholesterol-bound SCAP binds to insulin-induced gene 1 protein (INSIG1), promoting the settlement of the SREBP-SCAP complex on ER. When ER cholesterol falls below a critical threshold, SCAP undergoes a conformational change that allows the packaging of SREBP2-SCAP into COPII-encapsulated vesicles for subsequent transport to the Golgi. Compared with SCAP, functional studies of ERLIN2 are limited. It has been reported that the interaction of ERLIN2 with SREBP-SCAP-INSIG1 at ER is required to restrict SREBP activation under cholesterol-sufficient conditions (*34*). Our present study demonstrates that SNX10 is essential for the binding of ERLIN2 and SCAP to anchor the SREBP2 complex on ER. Therefore, manipulating the function or expression of SNX10 may be a possible way to restore the stemness of ISCs through SREBP2-mediated cholesterol synthesis.

In conclusion, we identify a critical role of SNX10 as an inherent restrictor in regulating the stemness of ISCs, and its expression

positively correlates with the severity of CD. Reducing SNX10 expression or inhibiting SNX10 function promoted mucosal healing by restoring the stemness of ISCs in colitis mice. Mechanism exploration revealed that the disassociation of ERLIN2 with SCAP by SNX10 deletion unlocked SREBP2 from ER and translocated it to Golgi for cleavage, resulting in SREBP2 activation for cholesterol biosynthesis. Our study elucidates that sufficient cholesterol is essential for the proliferation and differentiation of ISCs through the activation of the Wnt signaling pathway and therefore may be a new strategy for mucosal healing in CD. Targeting SNX10 or other regulators involved in SREBP cleavage or cholesterol metabolic axes to restore intestinal epithelial homeostasis will pave the way for the development of therapy for CD.

MATERIALS AND METHODS

Study design

This study was initiated to explore the role of SNX10 in CD. To achieve this aim, we used both experimental mouse models induced by DSS and published clinical datasets. For animal experiments, 8-week-old male mice of each genotype were allocated randomly for each experimental group, ensuring that the mean body weight in each group was similar. Experiments were performed in a nonblinded fashion. All animal experiments were performed under the auspices of the Experimental Animal Ethics Committee of the School of Pharmacy, Fudan University (approval number 2019-03-YL-SXY-01). Histopathological analyses, immunohistochemical staining, qPCR or RNA sequencing (RNA-seq), and measurement of proinflammatory cytokines in serum were performed to evaluate epithelium damage, quantification of specific cell populations, gene expression, and severity of inflammation. For in vitro experiments, we performed organoid cultures of epithelial cells isolated from the small intestine or colon of mice for assessing the effect of SNX10 KO on the self-renew of ISCs. The partial study of the molecular mechanism was established on human colon cancer cells HCT116 cell line to observe the intracellular localization of the protein of interest by fluorescence confocal microscopy.

Human samples

Sections for immunofluorescence staining were obtained from excised samples of colon or ileal lesions from patients with CD. The patients with CD were enrolled and followed up from July 2010 to July 2020 at the Department of Colorectal Surgery, Xinhua Hospital, Shanghai Jiao Tong University School of Medicine. CD diagnosis was based on clinical, endoscopic, and histologic criteria. The study complied with the Helsinki Declaration, and the study protocol was approved by the Institutional Ethics Committee of Xinhua Hospital affiliated with Shanghai Jiaotong University School of Medicine. All of the patients included in the study signed the informed consent.

Mice

Vil1-Cre and *Snx10-floxed* mice (C57Bl/6 background) were purchased from Shanghai Model Organisms Center Inc. (Shanghai, China). *Lgr5-EGFP-IRES-creERT2* mice were gifts from the Institute of Radiation Medicine, Fudan University (Shanghai, China). *Vil1-Cre* mice were mated with *Snx10-floxed* mice to generate $Snx10^{fl/fl}$;Cre^{-}(WT) and $Snx10^{fl/fl}$;$Vil\text{-}Cre^{+}$ ($Snx10^{\Delta IEC}$) mice. *Lgr5-EGFP-IRES-creERT2* mice were mated with *Snx10-floxed* mice to generate *Lgr5-EGFP-IRES-CreERT2*;$Snx10^{fl/fl}$ mice, which show tamoxifen-inducible KO of *Snx10* in LGR5^{+}ISCs; $Snx10^{\Delta ISC}$ refers to tamoxifen-induced *Lgr5-EGFP-IRES-CreERT2*;$Snx10^{fl/fl}$ mice, compared to *Lgr5-EGFP-IRES-CreERT2*;$Snx10^{fl/fl}$ mice without tamoxifen induction.

Cell culture

Human HCT116 cells purchased from American Type Culture Collection were cultured in low-glucose Dulbecco's modified Eagle's medium (DMEM) supplemented with 10% fetal bovine serum at 37°C under 5% (v/v) CO_2 atmosphere.

Crypt isolation and three-dimensional culture

Isolation of SI crypts was performed as previously described (*62*). Briefly, after euthanizing the mice, the ilea were opened longitudinally and washed with phosphate-buffered saline (PBS). Tissues were incubated at 4°C in EDTA (2 mM) for 30 min to dissociate the crypts which were suspended (200 to 400 crypts per well) in 50% Matrigel with a 50% advanced DMEM/F12 medium. After 20-min incubation to polymerize Matrigel, ENR medium containing advanced DMEM/F12, 2 mM GlutaMAX, 10 mM Hepes, Primocin (100 μg/ml), 1 mM N-acetyl cysteine, B27 supplement, N2 supplement, mouse EGF (20 ng/ml), mouse Noggin (100 ng/ml), and mouse R-spondin 1 (500 ng/ml) was added (*63*).

Colon organoid culture was modified from the previous protocol (*64*). Briefly, after euthanizing the mice, colons were opened longitudinally and washed with PBS. Tissues were incubated at 37°C in EDTA buffer (2 Mm EDTA, 43.4 mM sucrose, 54.9 mM D-sorbitol, and 0.5 mM DL-dithiothreitol) for 30 min to dissociate the crypts. The isolated crypts were incubated with TrypLE Express for 1 hour at 37°C to break up into individual cells. Colon epithelial cells were suspended in 50% Matrigel with a 50% advanced DMEM/F12 medium. After 20-min incubation to polymerize Matrigel, WENR was added.

Organoid measurement

For organoid size evaluation, the surface area of organoid horizontal cross sections was measured. Several random nonoverlapping pictures were acquired from each well by a Zeiss LSM 710 Observer Z1 inverted microscope, and then analyzed by ImageJ software. The "Analyze Particles" function of ImageJ software has been used to automatically determine the perimeter of organoids for area measurement. The threshold for organoid identification was set based on monochrome images. Organoids touching the edge of the images were excluded from the counting. On day 5 in culture, the SI organoid structure was scored manually under light microscopy based on the number of buds under light microscopy: sphere (no budding), organoid 1 (one bud), organoid 2 (two buds), and organoid 3+ (three or more buds). The percentage of organoids with a different number of buds relative to the total number of organoids was calculated. On day 5 in culture, total colon organoid numbers per well were counted manually under light microscopy to evaluate colony formation efficiency (*63*).

Immunostaining and immunohistochemistry

Organoids in the plates were fixed with 4% paraformaldehyde for 45 min at 4°C. Then, organoids were treated with PBS containing 10% goat serum, 10% dimethyl sulfoxide, and 2% Triton X-100 for 1 hour. HCT116 cells were fixed with 4% paraformaldehyde for 10 min at 4°C, permeated with 0.1% Triton X-100 for 10 min, and blocked with 10% goat serum (Gibco, 16210064) for 2 hours. Cells or organoids were then incubated with primary antibodies for 2 hours at room temperature. After washing three times with PBS, cells

or organoids were incubated with appropriate Alexa Fluor–labeled secondary antibodies in the blocking buffer for 2 hours at room temperature. The slides were sealed by mounting media containing 4′,6-diamidino-2-phenylindole, and then observed under a laser scanning confocal microscope (Zeiss, Germany) (*65*). Colocalization analysis was completed by ImageJ's JACop plugin.

Tissue samples were fixed in 4% paraformaldehyde and embedded in paraffin. Tissue embedding and sectioning assay were performed by Servicebio Inc. (Shanghai, China). For immunofluorescence staining, sections were deparaffinized with standard techniques, incubated with primary antibodies overnight at 4°C, and then incubated with secondary antibodies at room temperature for 30 min. H&E staining and IHC assay were performed by Servicebio Inc. (Shanghai, China). The H&E-stained sections of the colon were analyzed by a light microscope (Olympus, Japan) to quantify the number and length of complete crypts. The immunofluorescence and IHC staining sections of the colon were pictured by an inverted phase contrast fluorescence microscope (Olympus, Japan). Fluorescence images are processed and analyzed by ImageJ software.

In vivo experiments

All experiments based on the DSS model were performed on 8-week-old male mice, including a 6-day 3% DSS modeling process and a 3-day or longer recovery period of normal drinking water. For compound treatment, mice that received DSS were administered intragastrically once daily throughout the course (Fig. 7) or after the onset of symptoms (fig. S7). Mice were weighed and scored for DAI daily. DAI was assessed terminally by an unbiased observer using a previously published scoring system (*28*). Each mouse was scored from three aspects: rectal bleeding, stool consistency, and weight loss, each with a score of 0 to 4. On the indicated day, the mice were euthanized to collect colon tissues and blood. For the TNBS model, we adopted two strategies. For the experiments of DC-SX029 evaluation, we used a standard single-application TNBS model of 8-week-old female BALB/c mice. Briefly, mice were fasted for 24 hours before the experiment, and after ether anesthesia, a 2.0-mm-diameter syringe hose was lubricated with paraffin oil, gently inserted by the anus, and 200 μl of 5% TNBS/50% ethanol (1:1) solution was slowly injected (the normal control group was instilled with PBS solution), the tail was lifted, and the mice were kept lying flat and naturally awake after 5 min of continuous inversion, free to eat and drink. For transgenic mice with a C57BL/6 background, we added a presensitization step before modeling to increase the sensitivity of C57BL/6 mice to TNBS. After the mice were anesthetized, a 1.5-cm^2 area of hair between the shoulders of the back of the mice was shaved using an electric razor to expose the skin, 150 μl of 1% (w/v) TNBS presensitization fluid was applied to the shaved skin area using a pipette gun, and control mice were treated with the TNBS-free presensitization solution. After 6 days of presensitization, the mice were administered intrarectally with TNBS (*28*). Mice were grouped using a completely randomized method. According to the 3R principle, at least six mice were assigned to each group.

In vivo intestinal permeability assay

The intestinal barrier integrity was assessed using fluorescein isothiocyanate (FITC)–dextran as previously described (*66*). Briefly, mice were starved for 4 hours, and then gavaged with FITC-dextran (600 mg/kg) followed by 4-hour fasting before euthanization. The content of FITC-dextran in serum was measured according to the standard curve by a microplate reader at a 480-nm excitation wavelength and a 525-nm emission wavelength.

Isolation of colonic epithelial cells

Colonic epithelial cells were isolated using a protocol as described (*67*). Briefly, colon tissues from mice were opened longitudinally and flushed with ice-cold PBS. Tissues were cut into small pieces (1 cm) and vigorously shaken in Hanks' balanced salt solution containing 40 mM EDTA and 1 mM dithiothreitol at 37°C for 20 min, and then passed through a 100-μm cell strainer. Epithelial cells in the filtering liquid were collected and centrifuged at 300*g* for 10 min at 4°C. The isolated colonic epithelial cells were lysed followed by a WB or RT-qPCR measurement.

Construction of *SNX10* knockout stable cell line and reintroduction assay

The CRISPR-Cas9 system was used to generate *SNX10* KO stable HCT116 cell line. Small-guide RNA (sgRNA) targeting human *SNX10* sequence is GTGTCTGGGTTCGAGATCCT. Lentivirus (Lenti-CAS9-sgRNA-puro) encoding Cas9 and sgRNA targeting *SNX10* or the control vector were constructed and packed by GeneChem (Shanghai, China). Cultured HCT116 cells were infected by Lentivirus-CAS9-sgRNA-puromycin. After 72 hours, SNX10 KO cells were selected by puromycin and further confirmed by WB. For the reintroduction of SNX10, recombinant vector (EV-flag or SNX10-flag) were constructed and transfected into SNX10 KO cells with Lipofectamine 3000.

Immunoprecipitation

Cells transfected by SNX10-Flag plasmid were lysed in a buffer containing 50 mM tris-HCl, 1% NP-40, 150 mM NaCl, cocktail protease inhibitors (Roche, 04693116001), and 0.1% SDS-Na for 30 min, then centrifuged at 13,000*g* for 15 min. Cell lysates were incubated with 30 μl of anti-FLAG M2 agarose for 6 hours at 4°C. For endogenous proteins, the sample was incubated with the antibody or immunoglobulin G for 12 hours at 4°C, and then protein A/G agarose (70 to 100 μl) was added to each sample. The lysate beads mixture was incubated at 4°C under rotary agitation for 4 hours. Immunocomplexes were washed three times with 1 ml of lysis buffer and then detected by WB.

Western blot

Total proteins from cells or tissues were isolated by radioimmunoprecipitation assay buffer on ice. BCA Protein Assay Kit was used to determine the concentration of proteins. Equal amounts of proteins (10 to 60 μg) of each group were performed by the standard protocol of WB.

ELISA

The blood of mice was let stand for 2 hours and centrifuged for 15 min at 3000 rpm to collect serum. The samples above were analyzed for cytokine concentration with ELISA (enzyme-linked immunosorbent assay) kits according to the manufacturer's protocol (DAKEWE, Shanghai, China).

RNA isolation and RT-qPCR

For RT-qPCR analysis, the cells or tissues were lysed in TRIzol reagent to extract total RNA, followed by reverse transcription with HiScript II 1st Strand cDNA Synthesis Kit. Real-Time PCR was performed using Hieff UNICON qPCR SYBR Green Master Mix. All

primers used for qPCR analysis were synthesized by HuaGen Biotech (Shanghai, China). β-Actin or 18*S* ribosomal RNA was used as an internal control. All the qPCR primer sequences used in this study are listed in table S2.

RNA sequencing of colonic epithelial cells from colitis mice

The mRNA was purified from 1 μg of total RNA using oligo (dT) magnetic beads followed by fragmentation carried out using divalent cations at elevated temperatures. Subsequently, first-strand and second-strand cDNAs were synthesized, followed by PCR amplification. PCR products were purified (AMPure XP system), and library quality was assessed on an Agilent Bioanalyzer 4150 system. Last, sequencing was performed with an Illumina NovaSeq 6000/MGISEQ-T7 instrument. Raw reads of fastq format were first processed through in-house perl scripts. In this step, the adapter sequence, low-quality (low quality means the number of lines with a string quality value less than or equal to 25 accounts for more than 60% of the entire reading), and N (N means that the base information cannot be determined) ratio is greater than 5% reads that were removed to obtain clean reads that can be used for subsequent analysis. Then, clean reads were separately aligned to the reference genome with orientation mode using HISAT2 software (http://daehwankimlab.github.io/hisat2/) to obtain mapped reads. FeatureCounts (http://subread.sourceforge.net/) was used to count the reads numbers mapped to each gene. Then, the fragments per kilobase million (FPKM) of each gene was calculated on the basis of the length of the gene and reads count mapped to this gene. RNA-seq was performed by Applied Protein Technology (Shanghai, China).

GSEA and correlation analysis of datasets

RNA-seq results of colonic epithelial cells from colitis mice and the clinical data from the GSE112366 and GSE100833 datasets were performed standard GSEA and correlation analysis by using R (version 4.1.2). Nominal *P* values are shown.

Statistical analysis

Statistical analysis was done by GraphPad Prism 7. Unless otherwise indicated, data are represented as means ± SD; not significant (ns), $*P < 0.05$, $**P < 0.01$, and $***P < 0.001$. Differences in the quantitative data were analyzed using a two-tailed unpaired *t* test between two groups, one-way or two-way analysis of variance (ANOVA) followed by Bonferroni post hoc test for more than two groups. Survival curves were analyzed according to the log-rank (Mantel-Cox) test. Correlation between different data was performed by Spearman's correlation analysis.

Supplementary Materials

This PDF file includes:

Figs. S1 to S8
Tables S1 and S2

REFERENCES AND NOTES

1. M. F. Neurath, S. P. L. Travis, Mucosal healing in inflammatory bowel diseases: A systematic review. *Gut* **61**, 1619–1635 (2012).
2. J. Beumer, H. Clevers, Cell fate specification and differentiation in the adult mammalian intestine. *Nat. Rev. Mol. Cell Biol.* **22**, 39–53 (2021).
3. S. Khaloian, E. Rath, N. Hammoudi, E. Gleisinger, A. Blutke, P. Giesbertz, E. Berger, A. Metwaly, N. Waldschmitt, M. Allez, D. Haller, Mitochondrial impairment drives intestinal stem cell transition into dysfunctional Paneth cells predicting Crohn's disease recurrence. *Gut* **69**, 1939–1951 (2020).
4. R. Elmentaite, A. D. B. Ross, K. Roberts, K. R. James, D. Ortmann, T. Gomes, K. Nayak, L. Tuck, S. Pritchard, O. A. Bayraktar, R. Heuschkel, L. Vallier, S. A. Teichmann, M. Zilbauer, Single-Cell sequencing of developing human gut reveals transcriptional links to childhood Crohn's disease. *Dev. Cell* **55**, 771–783.e5 (2020).
5. K. Suzuki, T. Murano, H. Shimizu, G. Ito, T. Nakata, S. Fujii, F. Ishibashi, A. Kawamoto, S. Anzai, R. Kuno, K. Kuwabara, J. Takahashi, M. Hama, S. Nagata, Y. Hiraguri, K. Takenaka, S. Yui, K. Tsuchiya, T. Nakamura, K. Ohtsuka, M. Watanabe, R. Okamoto, Single cell analysis of Crohn's disease patient-derived small intestinal organoids reveals disease activity-dependent modification of stem cell properties. *J. Gastroenterol.* **53**, 1035–1047 (2018).
6. M. Kanke, M. M. Kennedy Ng, S. Connelly, M. Singh, M. Schaner, M. T. Shanahan, E. A. Wolber, C. Beasley, G. Lian, A. Jain, M. D. Long, E. L. Barnes, H. H. Herfarth, K. L. Isaacs, J. J. Hansen, M. Kapadia, J. G. Guillem, C. Feschotte, T. S. Furey, S. Z. Sheikh, P. Sethupathy, Single-cell analysis reveals unexpected cellular changes and transposon expression signatures in the colonic epithelium of treatment-naïve adult Crohn's disease patients. *Cell. Mol. Gastroenterol. Hepatol.* **13**, 1717–1740 (2022).
7. D. N. Jackson, M. Panopoulos, W. L. Neumann, K. Turner, B. L. Cantarel, L. Thompson-Snipes, T. Dassopoulos, L. A. Feagins, R. F. Souza, J. C. Mills, R. S. Blumberg, K. Venuprasad, W. E. Thompson, A. L. Theiss, Mitochondrial dysfunction during loss of prohibitin 1 triggers Paneth cell defects and ileitis. *Gut* **69**, 1928–1938 (2020).
8. C. W. Cheng, M. Biton, A. L. Haber, N. Gunduz, G. Eng, L. T. Gaynor, S. Tripathi, G. Calibasi-Kocal, S. Rickelt, V. L. Butty, M. Moreno-Serrano, A. M. Iqbal, K. E. Bauer-Rowe, S. Imada, M. S. Ulutas, C. Mylonas, M. T. Whary, S. S. Levine, Y. Basbinar, R. O. Hynes, M. Mino-Kenudson, V. Deshpande, L. A. Boyer, J. G. Fox, C. Terranova, K. Rai, H. Piwnica-Worms, M. M. Mihaylova, A. Regev, O. H. Yilmaz, Ketone body signaling mediates intestinal stem cell homeostasis and adaptation to diet. *Cell* **178**, 1115–1131. e15 (2019).
9. B. Wang, X. Rong, E. N. D. Palladino, J. Wang, A. M. Fogelman, M. G. Martin, W. A. Alrefai, D. A. Ford, P. Tontonoz, Phospholipid remodeling and cholesterol availability regulate intestinal stemness and tumorigenesis. *Cell Stem Cell* **22**, 206–220.e4 (2018).
10. V. Hrabovsky, Z. Zadak, V. Blaha, R. Hyspler, T. Karlik, A. Martinek, A. Mendlova, Cholesterol metabolism in active Crohn's disease. *Wien. Klin. Wochenschr.* **121**, 270–275 (2009).
11. R. S. R. Sappati Biyyani, B. S. Putka, K. D. Mullen, Dyslipidemia and lipoprotein profiles in patients with inflammatory bowel disease. *J. Clin. Lipidol.* **4**, 478–482 (2010).
12. H. Soh, J. P. Im, K. Han, S. Park, S. W. Hong, J. M. Moon, E. A. Kang, J. Chun, H. J. Lee, J. S. Kim, Crohn's disease and ulcerative colitis are associated with different lipid profile disorders: A nationwide population-based study. *Aliment. Pharmacol. Ther.* **51**, 446–456 (2020).
13. C. H. Zhu, L. R. Morse, R. A. Battaglino, SNX10 is required for osteoclast formation and resorption activity. *J. Cell. Biochem.* **113**, 1608–1615 (2012).
14. B. Qin, M. He, X. Chen, D. Pei, Sorting nexin 10 induces giant vacuoles in mammalian cells. *J. Biol. Chem.* **281**, 36891–36896 (2006).
15. X. Wang, J. Ni, Y. You, G. Feng, S. Zhang, W. Bao, H. Hou, H. Li, L. Liu, M. Zheng, Y. Wang, H. Zhou, W. Shen, X. Shen, SNX10-mediated LPS sensing causes intestinal barrier dysfunction via a caspase-5-dependent signaling cascade. *EMBO J.* **40**, e108080 (2021).
16. L. A. Peters, J. Perrigoue, A. Mortha, A. Iuga, W. M. Song, E. M. Neiman, S. R. Llewellyn, A. Di Narzo, B. A. Kidd, S. E. Telesco, Y. Zhao, A. Stojmirovic, J. Sendecki, K. Shameer, R. Miotto, B. Losic, H. Shah, E. Lee, M. Wang, J. J. Faith, A. Kasarskis, C. Brodmerkel, M. Curran, A. Das, J. R. Friedman, Y. Fukui, M. B. Humphrey, B. M. Iritani, N. Sibinga, T. K. Tarrant, C. Argmann, K. Hao, P. Roussos, J. Zhu, B. Zhang, R. Dobrin, L. F. Mayer, E. E. Schadt, A functional genomics predictive network model identifies regulators of inflammatory bowel disease. *Nat. Genet.* **49**, 1437–1449 (2017).
17. W. Bao, X. Liu, Y. You, H. Hou, X. Wang, S. Zhang, H. Li, G. Feng, X. Cao, H. Jiang, M. Zheng, X. Shen, Targeting sorting nexin 10 improves mouse colitis via inhibiting PIKfyve-mediated TBK1/c-Rel signaling activation. *Pharmacol. Res.* **169**, 105679 (2021).
18. Y. You, C. Zhou, D. Li, Z. L. Cao, W. Shen, W. Z. Li, S. Zhang, B. Hu, X. Shen, Sorting nexin 10 acting as a novel regulator of macrophage polarization mediates inflammatory response in experimental mouse colitis. *Sci. Rep.* **6**, 20630 (2016).
19. J. Padilla, N. T. Jenkins, P. K. Thorne, J. S. Martin, R. S. Rector, J. W. Davis, M. H. Laughlin, Identification of genes whose expression is altered by obesity throughout the arterial tree. *Physiol. Genomics* **46**, 821–832 (2014).
20. L. Lind, Genome-wide association study of the metabolic syndrome in UK biobank. *Metab. Syndr. Relat. Disord.* **17**, 505–511 (2019).
21. M. E. Cannon, K. W. Currin, K. L. Young, H. J. Perrin, S. Vadlamudi, A. Safi, L. Song, Y. Wu, M. Wabitsch, M. Laakso, G. E. Crawford, K. L. Mohlke, Open chromatin profiling in adipose tissue marks genomic regions with functional roles in cardiometabolic traits. *G3 (Bethesda)* **9**, 2521–2533 (2019).
22. C. Castillejo-Lopez, M. Pjanic, A. C. Pirona, S. Hetty, M. Wabitsch, C. Wadelius, T. Quertermous, E. Arner, E. Ingelsson, Detailed functional characterization of a waist-hip ratio locus in

7p15.2 defines an enhancer controlling adipocyte differentiation. *iScience* **20**, 42–59 (2019).
23. Y. You, W.-L. Bao, S.-L. Zhang, H.-D. Li, H. Li, W.-Z. Dang, S.-L. Zou, X.-Y. Cao, X. Wang, L.-X. Liu, H. Jiang, L.-F. Qu, M. Zheng, X. Shen, Sorting Nexin 10 mediates metabolic reprogramming of macrophages in atherosclerosis through the Lyn-dependent TFEB signaling pathway. *Circ. Res.* **127**, 534–549 (2020).
24. K. L. VanDussen, A. Stojmirovic, K. Li, T. C. Liu, P. K. Kimes, B. D. Muegge, K. F. Simpson, M. A. Ciorba, J. G. Perrigoue, J. R. Friedman, J. E. Towne, R. D. Head, T. S. Stappenbeck, Abnormal small intestinal epithelial microvilli in patients with Crohn's disease. *Gastroenterology* **155**, 815–828 (2018).
25. L. Jostins, S. Ripke, R. K. Weersma, R. H. Duerr, D. P. McGovern, K. Y. Hui, J. C. Lee, L. P. Schumm, Y. Sharma, C. A. Anderson, J. Essers, M. Mitrovic, K. Ning, I. Cleynen, E. Theatre, S. L. Spain, S. Raychaudhuri, P. Goyette, Z. Wei, C. Abraham, J. P. Achkar, T. Ahmad, L. Amininejad, A. N. Ananthakrishnan, V. Andersen, J. M. Andrews, L. Baidoo, T. Balschun, P. A. Bampton, A. Bitton, G. Boucher, S. Brand, C. Buning, A. Cohain, S. Cichon, M. D'Amato, D. De Jong, K. L. Devaney, M. Dubinsky, C. Edwards, D. Ellinghaus, L. R. Ferguson, D. Franchimont, K. Fransen, R. Gearry, M. Georges, C. Gieger, J. Glas, T. Haritunians, A. Hart, C. Hawkey, M. Hedl, X. Hu, T. H. Karlsen, L. Kupcinskas, S. Kugathasan, A. Latiano, D. Laukens, I. C. Lawrance, C. W. Lees, E. Louis, G. Mahy, J. Mansfield, A. R. Morgan, C. Mowat, W. Newman, O. Palmieri, C. Y. Ponsioen, U. Potocnik, N. J. Prescott, M. Regueiro, J. I. Rotter, R. K. Russell, J. D. Sanderson, M. Sans, J. Satsangi, S. Schreiber, L. A. Simms, J. Sventoraityte, S. R. Targan, K. D. Taylor, M. Tremelling, H. W. Verspaget, M. De Vos, C. Wijmenga, D. C. Wilson, J. Winkelmann, R. J. Xavier, S. Zeissig, B. Zhang, C. K. Zhang, H. Zhao; International IBD Genetics Consortium (IIBDGC), M. S. Silverberg, V. Annese, H. Hakonarson, S. R. Brant, G. Radford-Smith, C. G. Mathew, J. D. Rioux, E. E. Schadt, M. J. Daly, A. Franke, M. Parkes, S. Vermeire, J. C. Barrett, J. H. Cho, Host-microbe interactions have shaped the genetic architecture of inflammatory bowel disease. *Nature* **491**, 119–124 (2012).
26. B. Kremer, R. Mariman, M. van Erk, T. Lagerweij, L. Nagelkerken, Temporal colonic gene expression profiling in the recurrent colitis model identifies early and chronic inflammatory processes. *PLOS ONE* **7**, e50388 (2012).
27. S. J. Edmunds, N. C. Roy, M. Davy, J. M. Cooney, M. P. Barnett, S. Zhu, Z. Park, D. R. Love, W. A. Laing, Effects of kiwifruit extracts on colonic gene and protein expression levels in IL-10 gene-deficient mice. *Br. J. Nutr.* **108**, 113–129 (2012).
28. S. Wirtz, V. Popp, M. Kindermann, K. Gerlach, B. Weigmann, S. Fichtner-Feigl, M. F. Neurath, Chemically induced mouse models of acute and chronic intestinal inflammation. *Nat. Protoc.* **12**, 1295–1309 (2017).
29. K. Taniguchi, L. W. Wu, S. I. Grivennikov, P. R. de Jong, I. Lian, F. X. Yu, K. Wang, S. B. Ho, B. S. Boland, J. T. Chang, W. J. Sandborn, G. Hardiman, E. Raz, Y. Maehara, A. Yoshimura, J. Zucman-Rossi, K. L. Guan, M. Karin, A gp130-Src-YAP module links inflammation to epithelial regeneration. *Nature* **519**, 57–62 (2015).
30. H. Tian, B. Biehs, C. Chiu, C. W. Siebel, Y. Wu, M. Costa, F. J. de Sauvage, O. D. Klein, Opposing activities of Notch and Wnt signaling regulate intestinal stem cells and gut homeostasis. *Cell Rep.* **11**, 33–42 (2015).
31. J. Munoz, D. E. Stange, A. G. Schepers, M. van de Wetering, B.-K. Koo, S. Itzkovitz, R. Volckmann, K. S. Kung, J. Koster, S. Radulescu, K. Myant, R. Versteeg, O. J. Sansom, J. H. van Es, N. Barker, A. van Oudenaarden, S. Mohammed, A. J. R. Heck, H. Clevers, The Lgr5 intestinal stem cell signature: Robust expression of proposed quiescent '+4' cell markers. *EMBO J.* **31**, 3079–3091 (2012).
32. R. Sheng, H. Kim, H. Lee, Y. Xin, Y. Chen, W. Tian, Y. Cui, J. C. Choi, J. Doh, J. K. Han, W. Cho, Cholesterol selectively activates canonical Wnt signalling over non-canonical Wnt signalling. *Nat. Commun.* **5**, 4393 (2014).
33. C. M. Adams, J. Reitz, J. K. De Brabander, J. D. Feramisco, L. Li, M. S. Brown, J. L. Goldstein, Cholesterol and 25-hydroxycholesterol inhibit activation of SREBPs by different mechanisms, both involving SCAP and Insigs. *J. Biol. Chem.* **279**, 52772–52780 (2004).
34. M. D. Huber, P. W. Vesely, K. Datta, L. Gerace, Erlins restrict SREBP activation in the ER and regulate cellular cholesterol homeostasis. *J. Cell Biol.* **203**, 427–436 (2013).
35. T. Xu, J. Xu, Y. Ye, Q. Wang, X. Shu, D. Pei, J. Liu, Structure of human SNX10 reveals insights into its role in human autosomal recessive osteopetrosis. *Proteins* **82**, 3483–3489 (2014).
36. R. Yan, P. Cao, W. Song, H. Qian, X. Du, H. W. Coates, X. Zhao, Y. Li, S. Gao, X. Gong, X. Liu, J. Sui, J. Lei, H. Yang, A. J. Brown, Q. Zhou, C. Yan, N. Yan, A structure of human Scap bound to Insig-2 suggests how their interaction is regulated by sterols. *Science* **371**, eabb2224 (2021).
37. S. Zhang, Z. Yang, W. Bao, L. Liu, Y. You, X. Wang, L. Shao, W. Fu, X. Kou, W. Shen, C. Yuan, B. Hu, W. Dang, K. S. Nandakumar, H. Jiang, M. Zheng, X. Shen, SNX10 (sorting nexin 10) inhibits colorectal cancer initiation and progression by controlling autophagic degradation of SRC. *Autophagy* **16**, 735–749 (2020).
38. I. Dotti, R. Mora-Buch, E. Ferrer-Picon, N. Planell, P. Jung, M. C. Masamunt, R. F. Leal, J. Martin de Carpi, J. Llach, I. Ordas, E. Batlle, J. Panes, A. Salas, Alterations in the epithelial stem cell compartment could contribute to permanent changes in the mucosa of patients with ulcerative colitis. *Gut* **66**, 2069–2079 (2017).
39. C. S. Smillie, M. Biton, J. Ordovas-Montanes, K. M. Sullivan, G. Burgin, D. B. Graham, R. H. Herbst, N. Rogel, M. Slyper, J. Waldman, M. Sud, E. Andrews, G. Velonias, A. L. Haber, K. Jagadeesh, S. Vickovic, J. Yao, C. Stevens, D. Dionne, L. T. Nguyen, A. C. Villani, M. Hofree, E. A. Creasey, H. Huang, O. Rozenblatt-Rosen, J. J. Garber, H. Khalili, A. N. Desch, M. J. Daly, A. N. Ananthakrishnan, A. K. Shalek, R. J. Xavier, A. Regev, Intra- and inter-cellular rewiring of the human colon during ulcerative colitis. *Cell* **178**, 714–730.e22 (2019).
40. N. Girish, C. Y. Liu, S. Gadeock, M. L. Gomez, Y. Huang, Z. Sharifkhodaei, M. K. Washington, D. B. Polk, Persistence of Lgr5+ colonic epithelial stem cells in mouse models of inflammatory bowel disease. *Am. J. Physiol. Gastrointest. Liver Physiol.* **321**, G308–G324 (2021).
41. C. Harnack, H. Berger, A. Antanaviciute, R. Vidal, S. Sauer, A. Simmons, T. F. Meyer, M. Sigal, R-spondin 3 promotes stem cell recovery and epithelial regeneration in the colon. *Nat. Commun.* **10**, 4368 (2019).
42. S. Yui, T. Nakamura, T. Sato, Y. Nemoto, T. Mizutani, X. Zheng, S. Ichinose, T. Nagaishi, R. Okamoto, K. Tsuchiya, H. Clevers, M. Watanabe, Functional engraftment of colon epithelium expanded in vitro from a single adult $Lgr5^+$ stem cell. *Nat. Med.* **18**, 618–623 (2012).
43. D. Castillo-Azofeifa, E. N. Fazio, R. Nattiv, H. J. Good, T. Wald, M. A. Pest, F. J. de Sauvage, O. D. Klein, S. Asfaha, $Atoh1^+$ secretory progenitors possess renewal capacity independent of $Lgr5^+$ cells during colonic regeneration. *EMBO J.* **38**, e99984 (2019).
44. G. M. H. Birchenough, M. E. V. Johansson, J. K. Gustafsson, J. H. Bergstrom, G. C. Hansson, New developments in goblet cell mucus secretion and function. *Mucosal Immunol.* **8**, 712–719 (2015).
45. J. Yi, K. Bergstrom, J. Fu, X. Shan, J. M. McDaniel, S. McGee, D. Qu, C. W. Houchen, X. Liu, L. Xia, Dclk1 in tuft cells promotes inflammation-driven epithelial restitution and mitigates chronic colitis. *Cell Death Differ.* **26**, 1656–1669 (2019).
46. M. El-Salhy, K. Umezawa, J. G. Hatlebakk, O. H. Gilja, Abnormal differentiation of stem cells into enteroendocrine cells in rats with DSS-induced colitis. *Mol. Med. Rep.* **15**, 2106–2112 (2017).
47. S. Yui, L. Azzolin, M. Maimets, M. T. Pedersen, R. P. Fordham, S. L. Hansen, H. L. Larsen, J. Guiu, M. R. P. Alves, C. F. Rundsten, J. V. Johansen, Y. Li, C. D. Madsen, T. Nakamura, M. Watanabe, O. H. Nielsen, P. J. Schweiger, S. Piccolo, K. B. Jensen, YAP/TAZ-dependent reprogramming of colonic epithelium links ECM remodeling to tissue regeneration. *Cell Stem Cell* **22**, 35–49.e7 (2018).
48. J. A. M. Sleutjes, J. E. Roeters van Lennep, C. J. van der Woude, A. C. de Vries, Lipid changes after induction therapy in patients with inflammatory bowel disease: Effect of different drug classes and inflammation. *Inflamm. Bowel Dis.* **29**, 531–538 (2023).
49. I. E. Koutroubakis, P. Oustamanolakis, N. Malliaraki, K. Karmiris, I. Chalkiadakis, E. Ganotakis, N. Karkavitsas, E. A. Kouroumalis, Effects of tumor necrosis factor alpha inhibition with infliximab on lipid levels and insulin resistance in patients with inflammatory bowel disease. *Eur. J. Gastroenterol. Hepatol.* **21**, 283–288 (2009).
50. E. Parmentier-Decrucq, A. Duhamel, O. Ernst, C. Fermont, A. Louvet, G. Vernier-Massouille, A. Cortot, J. F. Colombel, P. Desreumaux, L. Peyrin-Biroulet, Effects of infliximab therapy on abdominal fat and metabolic profile in patients with Crohn's disease. *Inflamm. Bowel Dis.* **15**, 1476–1484 (2009).
51. R. R. Stine, A. P. Sakers, T. TeSlaa, M. Kissig, Z. E. Stine, C. W. Kwon, L. Cheng, H. W. Lim, K. H. Kaestner, J. D. Rabinowitz, P. Seale, PRDM16 maintains homeostasis of the intestinal epithelium by controlling region-specific metabolism. *Cell Stem Cell* **25**, 830–845.e8 (2019).
52. M. M. Mihaylova, C. W. Cheng, A. Q. Cao, S. Tripathi, M. D. Mana, K. E. Bauer-Rowe, M. Abu-Remaileh, L. Clavain, A. Erdemir, C. A. Lewis, E. Freinkman, A. S. Dickey, A. R. La Spada, Y. Huang, G. W. Bell, V. Deshpande, P. Carmeliet, P. Katajisto, D. M. Sabatini, O. H. Yilmaz, Fasting activates fatty acid oxidation to enhance intestinal stem cell function during homeostasis and aging. *Cell Stem Cell* **22**, 769–778.e4 (2018).
53. P. Lochhead, H. Khalili, M. C. Sachs, A. T. Chan, O. Olén, J. F. Ludvigsson, Association between statin use and inflammatory bowel diseases: Results from a Swedish, nationwide, population-based case-control study. *J. Crohns Colitis* **15**, 757–765 (2021).
54. A. S. Bhagavathula, C. Clark, J. Rahmani, Statin use and new-onset of inflammatory bowel disease: A systematic review and meta-analysis of over ten million participants. *Eur. J. Pharmacol.* **891**, 173750 (2021).
55. O. Grip, S. Janciauskiene, A. Bredberg, Use of atorvastatin as an anti-inflammatory treatment in Crohn's disease. *Br. J. Pharmacol.* **155**, 1085–1092 (2008).
56. Y. Abe, M. Murano, N. Murano, E. Morita, T. Inoue, K. Kawakami, K. Ishida, T. Kuramoto, K. Kakimoto, T. Okada, K. Narabayashi, E. Umegaki, K. Higuchi, Simvastatin attenuates intestinal fibrosis independent of the anti-inflammatory effect by promoting fibroblast/myofibroblast apoptosis in the regeneration/healing process from TNBS-induced colitis. *Dig. Dis. Sci.* **57**, 335–344 (2012).
57. Y. Naito, K. Katada, T. Takagi, H. Tsuboi, Y. Isozaki, O. Handa, S. Kokura, N. Yoshida, H. Ichikawa, T. Yoshikawa, Rosuvastatin, a new HMG-CoA reductase inhibitor, reduces the

colonic inflammatory response in dextran sulfate sodium-induced colitis in mice. *Int. J. Mol. Med.* **17**, 997–1004 (2006).
58. M. Ikeda, F. Takeshima, H. Isomoto, S. Shikuwa, Y. Mizuta, Y. Ozono, S. Kohno, Simvastatin attenuates trinitrobenzene sulfonic acid-induced colitis, but not oxazalone-induced colitis. *Dig. Dis. Sci.* **53**, 1869–1875 (2008).
59. P. Duewell, H. Kono, K. J. Rayner, C. M. Sirois, G. Vladimer, F. G. Bauernfeind, G. S. Abela, L. Franchi, G. Nunez, M. Schnurr, T. Espevik, E. Lien, K. A. Fitzgerald, K. L. Rock, K. J. Moore, S. D. Wright, V. Hornung, E. Latz, NLRP3 inflammasomes are required for atherogenesis and activated by cholesterol crystals. *Nature* **464**, 1357–1361 (2010).
60. L. D. Lazaridis, A. Pistiki, E. J. Giamarellos-Bourboulis, M. Georgitsi, G. Damoraki, D. Polymeros, G. D. Dimitriadis, K. Triantafyllou, Activation of NLRP3 inflammasome in inflammatory bowel disease: Differences between crohn's disease and ulcerative colitis. *Dig. Dis. Sci.* **62**, 2348–2356 (2017).
61. C. Bauer, P. Duewell, C. Mayer, H. A. Lehr, K. A. Fitzgerald, M. Dauer, J. Tschopp, S. Endres, E. Latz, M. Schnurr, Colitis induced in mice with dextran sulfate sodium (DSS) is mediated by the NLRP3 inflammasome. *Gut* **59**, 1192–1199 (2010).
62. T. Sato, R. G. Vries, H. J. Snippert, M. van de Wetering, N. Barker, D. E. Stange, J. H. van Es, A. Abo, P. Kujala, P. J. Peters, H. Clevers, Single Lgr5 stem cells build crypt-villus structures in vitro without a mesenchymal niche. *Nature* **459**, 262–265 (2009).
63. C. A. Lindemans, M. Calafiore, A. M. Mertelsmann, M. H. O'Connor, J. A. Dudakov, R. R. Jenq, E. Velardi, L. F. Young, O. M. Smith, G. Lawrence, J. A. Ivanov, Y. Y. Fu, S. Takashima, G. Hua, M. L. Martin, K. P. O'Rourke, Y. H. Lo, M. Mokry, M. Romera-Hernandez, T. Cupedo, L. Dow, E. E. Nieuwenhuis, N. F. Shroyer, C. Liu, R. Kolesnick, M. R. M. van den Brink, A. M. Hanash, Interleukin-22 promotes intestinal-stem-cell-mediated epithelial regeneration. *Nature* **528**, 560–564 (2015).
64. T. Sato, D. E. Stange, M. Ferrante, R. G. J. Vries, J. H. Van Es, S. Van den Brink, W. J. Van Houdt, A. Pronk, J. Van Gorp, P. D. Siersema, H. Clevers, Long-term expansion of epithelial organoids from human colon, adenoma, adenocarcinoma, and Barrett's epithelium. *Gastroenterology* **141**, 1762–1772 (2011).
65. M. J. Rodriguez-Colman, M. Schewe, M. Meerlo, E. Stigter, J. Gerrits, M. Pras-Raves, A. Sacchetti, M. Hornsveld, K. C. Oost, H. J. Snippert, N. Verhoeven-Duif, R. Fodde, B. M. T. Burgering, Interplay between metabolic identities in the intestinal crypt supports stem cell function. *Nature* **543**, 424–427 (2017).
66. G. Chen, X. Ran, B. Li, Y. Li, D. He, B. Huang, S. Fu, J. Liu, W. Wang, Sodium butyrate inhibits inflammation and maintains epithelium barrier integrity in a TNBS-induced inflammatory bowel disease mice model. *EBioMedicine* **30**, 317–325 (2018).
67. B. Weigmann, I. Tubbe, D. Seidel, A. Nicolaev, C. Becker, M. F. Neurath, Isolation and subsequent analysis of murine lamina propria mononuclear cells from colonic tissue. *Nat. Protoc.* **2**, 2307–2311 (2007).

Acknowledgments: We thank H. Guoqiang for providing *Lgr5-EGFP-IRES-creERT2* mouse lines. **Funding:** This work was supported by the National Natural Science Foundation of China (no. 82130108), National Natural Science Foundation of China (no. 82174044), National Natural Science Foundation of China (no. 81773744), Shanghai Science and Technology Innovation Action Plan experimental animal research project (no. 19140901800), National Health and Medical Research Council (NHMRC) of Australia (APP1163933), and China Postdoctoral Science Foundation (nos. BX20220069 and 2021M700864). **Author contributions:** Conceptualization: W.B., Y.Y., Ho.L., X.L., P.D., D.C., and X.S. Methodology: W.B., J.N., H.H., S.Z., J.L., K.Y., G.F., Y.W., X.C., X.W., and Ha.L. Investigation: W.B., J.N., H.H., J.L., K.Y., G.F., Y.W., X.C., X.W., and Ha.L. Visualization: W.B., L.Z., and G.F. Funding acquisition: W.B., Ho.L., J.X., X.L., D.C., and X.S. Project administration: X.L., P.D., D.C., and X.S. Supervision: X.L., P.D., D.C., and X.S. Resource: C.L. and P.D. Writing—original draft: W.B. and G.F. Writing—review and editing: W.B., Y.Y., D.C., and X.S. **Competing interests:** The authors declare that they have no competing interests. **Data and materials availability:** All data needed to evaluate the conclusions in the paper are present in the paper and/or the Supplementary Materials. RNA-seq data appearing in this paper have been deposited at SRA. The accession number of RNA-seq data is PRJNA881633/SRP397853. Accession numbers of published clinical data are GSE112366, GSE100833, GSE35609, and GSE27684.

Submitted 7 March 2023
Accepted 28 July 2023
Published 30 August 2023
10.1126/sciadv.adh5016